Coordination Chemistry Reviews 254 (2010) 355–371

Contents lists available at ScienceDirect

Coordination Chemistry Reviews

journal homepage: www.elsevier.com/locate/ccr

Review

Immobilized ruthenium complexes and aspects of their reactivity

Elia Tfouni[a,*], Fabio Gorzoni Doro[a,1], Anderson Jesus Gomes[a,2], Roberto Santana da Silva[b,**], Gustavo Metzker[c], Patricia Graça Zanichelli Benini[c], Douglas Wagner Franco[c,***]

[a] Departamento de Química, Faculdade de Filosofia, Ciências e Letras de Ribeirtão Preto, Universidade de São Paulo, Av. dos Bandeirantes, 3900, 14040-901 Ribeirão Preto, SP, Brazil
[b] Faculdade de Ciências Farmacêuticas de Ribeirão Preto, Universidade de São Paulo, Av. do Café s/n, 14040-903 Ribeirão Preto, SP, Brazil
[c] Instituto de Química de São Carlos, Universidade de São Paulo, Av. Trabalhador São-carlense, 400, 13566-590 São Carlos, SP, Brazil

Contents

ARTICLE INFO

Article history:
Received 28 May 2009
Accepted 17 October 2009
Available online 29 October 2009

ABSTRACT

Methodologies for the immobilization and characterization of ruthenium complexes into/onto functionalized silica gel, zeolites, polymers, dendrimers, sol–gel, nano and microparticles are described. The corresponding spectroscopic, electrochemical, and photochemical properties as well as chemical

Abbreviations: [15]aneN$_4$, 1,4,8,12-tetraazacyclopentadecane; bpy, 2,2′-bipyridine; cyclam, 1,4,8,11-tetraazacyclotetradecane; DCC, N,N′-dicyclohexylcarbodiimide; DCM, dichloromethane; DDS, drug delivery system; DMF, dimethylformamide; dpp, diphenylphosphine; dtdp, 4,4′-dithiopyridine; GLU, glutaraldehyde; G$_x$/Ru, PAMAM dendrimer modified with K[Ru(H$_2$O)(Hedta)]; G$_x$/RuNO, PAMAM dendrimer modified with [Ru(NO)(Hedta)]; Hedta, ethylenediamine tetraacetic acid; im*N*, nitrogen bound imidazole; isn, isonicotinamide; MP, microparticle; NHE, normal hydrogen electrode; NH.NHq, 3,4-diiminobenzoic acid; PAMAM, polyamidoamine dendrimers; PDMS, polydimethylsiloxane; PGA, poly(glycolic acid); 4-pic, 4-picoline; PLA, poly(lactic acid); PLGA, poly(lactic-co-glycolic) acid; PMA, poly(methylmethacrylate); P(OEt)$_3$, triethylphosphite; PU, polyurethane; PVA, poly(vinyl alcohol); PVC, poly(vinyl chloride); 4-PVP, 4-polyvinylpyridine; py, pyridine; pyMP, *trans*-[Ru(NO)(NH$_3$)$_4$(py)](BF$_4$)$_3$ loaded into PLGA microparticles; pz, pyrazine; salen, *N*,*N*′-bis-(salicylidene)ethylenediaminato; ≡Si(AEATS), silica gel modified with [3-(2-aminoethyl)aminopropyl]trimethoxysilane; ≡Si(CH$_2$)$_3$isn, silica gel modified with isonicotinamidepropyl groups; ≡Si(CH$_2$)$_3$NH$_2$, silica gel modified with aminopropyltrimethoxysilane; ≡SiOTi, silica gel modified with titanium; SiPr, (n-propyl)trimethoxysilane; SiSH, (3-mercaptopropyl)trimethoxysilane; Succ, N-hydroxysuccinimide; TEOS, Tetraethylorthosilicate; terpy, 2,2′:6′,2″-terpyridine; tfms, trifluoromethanesulfonic anion.

* Corresponding author. Tel.: +55 16 36023748.
** Corresponding author. Tel.: +55 16 36024428.
*** Corresponding author. Tel.: +55 16 33739970.
E-mail addresses: eltfouni@usp.br (E. Tfouni), fabiodoro@ufba.br (F.G. Doro), ajgomes@unb.br (A.J. Gomes), silva@usp.br (R.S.d. Silva), douglas@iqsc.usp.br (D.W. Franco).
[1] Present address: Instituto de Química, Universidade Federal da Bahia, Rua Barão de Geremoabo, 147, 40170-290 Salvador, BA, Brazil. Tel.: +55 71 32836878.
[2] Present address: Universidade de Brasília, Faculdade Ceilândia, QNN 14 AE-CEI, 72220-140 Brasília, DF, Brazil. Tel.: +55 61 33766042.

0010-8545/$ – see front matter
doi:10.1016/j.ccr.2009.10.011

Keywords:
Ruthenium complexes
Immobilization
Silica
Silica gel
Xerogel
Zeolites
Membranes
Hydrogel
Micro and nanoparticles
Reactivity

reactivities are used for their characterization and study. Comparison between the reactivities of immobilized and in solution species is presented. Some biological applications are also described.

1. Introduction

Immobilization of coordination metal complexes onto/into matrices is an excellent approach for the preparation of sensors, catalysts, biomaterials, and drug transport and delivery systems [1–28], among others. A wide range of materials can be used as matrices, including inorganic and organic polymers such as silica [1–5,7,20,29–31], xerogels [21,32–34], organic inorganic hybrid materials [34,35], silicone rubbers [36], polyurethane (PU) [16,36], poly(vinyl chloride) (PVC) [37], poly(vinyl alcohol) (PVA) [36,38–42], poly(lactic-co-glycolic) acid (PLGA) [14], poly(methylmethacrylate) (PMA) [43] and dendrimers [6,44]. In addition, most of these materials can be made and/or modified, thereby resulting in different forms and shapes like powders, thin films, monoliths, nano or microparticles, and fibers [14,33,36,41,45–47], which can serve as a platform for the immobilization of metal coordination compounds. Supramolecular chemistry and photochemistry devoted to energy conversion and devices constitute other important fields of application of materials containing incorporated metal complexes. Another example of growing importance is the immobilization of nitric oxide (NO) donors, since NO and NO_x species are involved in a myriad of physiological processes and pathologies and may be either beneficial or harmful, depending on their bioavailability [48–51]. Consequently, several works devoted to the immobilization of NO donors, such as diazeniumdiolates [37,52–54] and transition metal nitrosyl complexes [15,20,21,32,55], which may lead to controlled NO bioavailability, have been reported. Among NO carriers, ruthenium nitrosyl complexes constitute a very interesting class and have been extensively studied over the past years for their novel biological and environmental reactivities [56–65]. In this sense, on one hand, due to the nitric oxide releasing properties of ruthenium nitrosyls, immobilization of this class of compounds may constitute a suitable approach for the preparation of drug delivery systems (DDS) capable of delivering NO to specific sites. The immobilization may provide further tuning for NO (or complex) release, with additional control of the accessibility of the nitrosyl complex to reduction sites. On the other hand, compounds can show key challenges when moving from solution to confined and surface immobilized systems. In this contribution, several approaches for immobilization of Ru complexes systems, particularly those developed in our Laboratories, are described and discussed using selected examples. The effect of the immobilization of these complexes on their chemical, electrochemical, photochemical, and reactivity properties is discussed here.

2. Immobilization procedures

The immobilization of ruthenium complexes onto/into solid materials can be performed by several methods commonly used for other metallic complexes or even other species, such as dyes [43,66,67]. The choice of the immobilization procedure depends on the structure of the complex, the material characteristics, and the desired properties. Complex–matrix coupling by covalent bonding [6,7], coordinative bonding [3,4,19,20] or electrostatic interactions [1], is generally applied for surface immobilization purposes. Immobilization into the backbone of a polymeric material, which may be achieved by simple dispersion of the species into the polymer or its precursor, prior to the polymerization process, does not require the formation of a covalent bond between the complex and the matrix. Such processes are largely applied in the preparation of xerogel materials doped with metallic complexes [21,32]. In addition, polymer precursors or complexes can be modified with functional groups and co-polymerized [55]. Some of these methods will be discussed below.

2.1. Silica gel

Silica gel is widely used as a supporting material because of its desirable properties such as mechanical and thermal resistance [29]. The silica gel surface, basically composed of silanol groups, can react with a wide range of compounds [29,30,68]. This is well illustrated by the extensive number of proposed reactions for chemically functionalized silica gel, which encompasses both inorganic and organic reactions [30]. For example, the reaction of an appropriate organosilicon compound, via the stable Si-O-Si-C moiety or metal alkoxide reaction with the silica surface [69], can form a layer of desirable specific functional groups that will promote interaction with the complex of interest.

Synthesis of functionalized silica gel has most commonly been achieved by successive reactions with modifying agents. Some examples are reported in Scheme 1, where R = 3-(2-aminoethyl)aminopropyl [7,70], aminopropyl [68] or 3-chloropropyl. Eqs. (1) and (2) show silica functionalization reaction with tetrabutyl orthotitanate [31].

$$n(\equiv \mathrm{SiOH}) + \mathrm{Ti(OR)_4} \rightleftharpoons (\equiv \mathrm{SiOH})n\mathrm{Ti(OR)_{(4-n)}} + n\mathrm{HOR} \quad (1)$$

$$(\equiv \mathrm{SiO})_n\mathrm{Ti(OR)_{(4-n)}} + (4-n)\mathrm{H_2O} \underset{\mathrm{OR=butoxi\ group}}{\rightleftharpoons} (\equiv \mathrm{SiO})_n\mathrm{Ti(OH)_{(4-n)}} + (4-n)\mathrm{HOR} \quad (2)$$

Ru and Os have great affinity for heterocyclic nitrogen molecules such as imidazole and isonicotinamide, and phosphorus(III) compounds, like chlorodiphenylphosphine. Therefore, the presence of these moieties in the modified silica should provide quite interesting supports for Ru and Os complexes. So, selected ligands can be used to functionalize the silica as represented in Eqs. (3) and (4) [3,20] For clarity, the silicon from the silica gel (SiO_2) has been

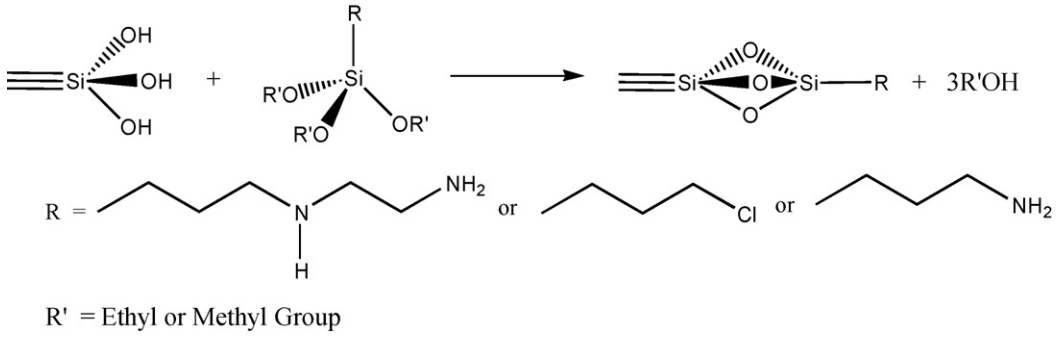

Scheme 1. Functionalization reactions of silica gel.

omitted from the equations below.

$$\equiv Si(CH_2)_3NH_2 + Cl{-}P(Ph)_2 \longrightarrow \equiv Si(CH_2)_3N(H){-}P(Ph)_2 + HCl \quad (3)$$

Ph = phenyl group

$$\equiv Si(CH_2)_3NH_2 + HO_2C\text{-}(C_5H_4N) \xrightarrow[DMF]{DCC} \equiv Si(CH_2)_3N(H)\text{-}C(=O)\text{-}(C_5H_4N) \quad (4)$$

Also, the desired ligand can first react with the silane functionalization agent followed by reaction with the silica gel surface, as in the case of the 3-(1-imidazolyl)-propyl functionalized silica gel [4] Eq. (5).

$$\equiv Si(OH)_3 + (CH_3O)_3Si(CH_2)_3(imN) \rightarrow \equiv Si(CH_2)_3(imN) + 3CH_3OH \quad (5)$$

In the sequence, the functionalized silica is reacted with the desired complex [3,4,20,31], as shown in Eqs. (6)–(8) and Scheme 2.

$$\equiv Si(CH_2)_3L + \textit{trans}\text{-}[Ru(SO_3)(NH_3)_4(H_2O)]^{+} \xrightarrow[pH=9.0]{NaHCO_3(aq)} [\equiv Si(CH_2)_3(L)Ru(SO_3)(NH_3)_4]^{+} + H_2O \quad (6)$$

$$(\equiv SiO)_nTi(OH)_{4-n} + [M(NH_3)_4(L)]^{n+} \xrightarrow[M=Ru^{III/II};\ Os^{III}]{} [\equiv (SiO)_nTi(O)M(NH_3)_5]^{n+} + L \quad (7)$$

$$\equiv Si(CH_2)_3N(H){-}P(Ph)_2 + [M(NH_3)_4(L)L']^{n+} \longrightarrow [\equiv Si(CH_2)_3N(H){-}P(Ph)_2{-}M(NH_3)_4(L')] + L \quad (8)$$

$M = Ru^{III/II}$; Ph = phenyl group; $L = SO_2$ or SO_3^{2-}; $L' = H_2O$

The approach for the synthesis of ruthenium ammine complexes in solution [71] following the SO_2/SO_4^{2-} pathway, was adapted for the immobilized complexes as shown in Scheme 2.

The SO_2/SO_4^{2-} pathway is preceeded by SO_3^{2-}/SO_2 aqueous equilibrium [72]. At pH values above 9.0 *trans*-$[Ru(SO_3)(NH_3)_4(OH_2)]$ predominates which allows formation of Ru-L(support) bonds due to the water lability in the Ru(II) complex, thereby leading to an immobilized sulfito complex. Lowering the pH, results in the formation of the sulfur dioxide complex which is oxidized to Ru(III) sulfate. It is known that reduction of Ru(III) tetraamine sulfato complexes results in fast aquation of the SO_4^{2-} ligand, with formation of the corresponding aquo Ru(II) complex [71,73].

The coordinative bonding described above may offer an additional advantage since the ligand attached to the surface can be changed, in order to obtain immobilized ruthenium ammine complexes other than those reported here. Except for where L′ and/or L = saturated ligands such as H_2O or Cl^- in *trans*-$[Ru^{II}(NH_3)_4LL']^{n+}$, which are kinetically labile, the Ru(II) and Ru(III) ammine complexes, *trans*-$[Ru(NH_3)_4LL']^{n+}$ are robust and thermodynamically stable [74,75]. Such a property allows the formation of a strong bond between the ruthenium ammine complex and the support, thus preventing leaching of the complex during manipulations.

The ruthenium load values for the immobilized $[\equiv Si(CH_2)_3LRu(NH_3)_4L']^{n+}$ (for L = im*N*, L′ = SO_3^{2-}, H_2O, pz, isn, or CO; for L = isn, L′ = SO_3^{2-}, SO_2, SO_4^{2-}, H_2O, or NO) are in the range of 2.0 to 4.0×10^{-4} mol of Ru per gram of silica support [4,20]. The average distance between the metal centers on the silica surface for the immobilized $[\equiv Si(CH_2)_3LRu(NH_3)_4L']^{n+}$ species estimated from the ruthenium load values are 6.6 and 15 Å for L′ = im*N* and isn, respectively [4,20]. Since the amount (1.3 to 2.2×10^{-5} mol per gram of silica) of immobilized metals in the $[\equiv SiTi(O)M(NH_3)_5]^{2+}$ system [31] is around 10 times lower than the one observed for the $[\equiv Si(CH_2)_3LRu(NH_3)_4L']^{n+}$ the calculated average distances between the metal centers are larger (ca. 59–64 Å for Ru and Os, respectively).

Based on ruthenium determinations after each step of functionalization, metal leaching during preparation is below 5% of the initial amount which is in agreement with the stability of the immobilized complexes [4,19,20,31]. On one hand, the load has a narrow range, determined by the number of available active coordination sites. But, on the other hand, these materials are very stable and, since the active groups are located on the surface, they offer ready access to reactions. This makes these materials easily recyclable, and, hence, important for catalytic activities.

Another synthetic approach uses a metal complex with an available unbound carboxylic group present in the coordinated ligands, such as EDTA in K[Ru(Cl)(Hedta)]. So, the immobiliztion reaction

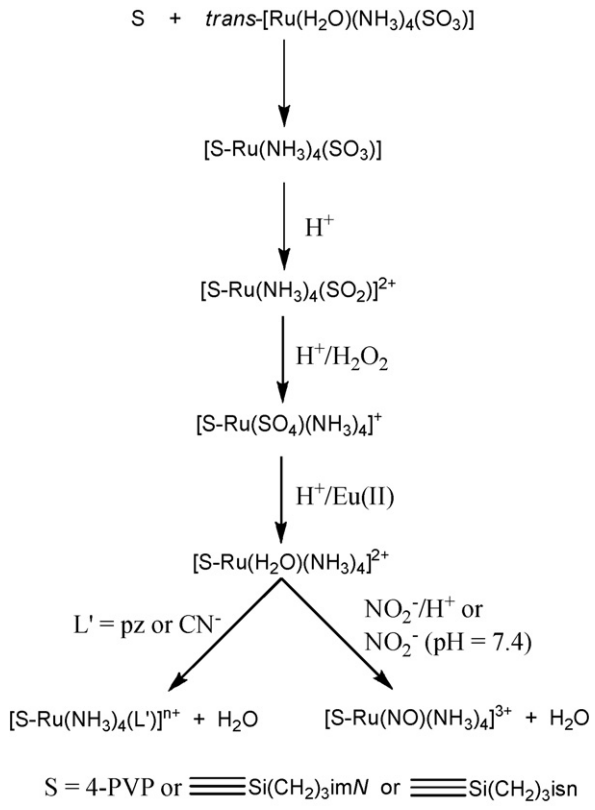

Scheme 2. Synthetic route for obtention of ruthenium tetraammines immobilized in modified surfaces using the SO_2/SO_4^{2-} pathway.

could be carried out directly with the functionalized silica surface, as follows [7]:

$$\equiv Si(CH_2)_3NH(CH_2)_2NH_2 + [M{-}COOH]^+ \xrightarrow[DMF]{DCC} [\equiv Si(CH_2)_3NH(CH_2)_2N(H){-}C(=O){-}M]^+ + H_2O$$

M = K[RuClHedta] (9)

The amide bond generated by this reaction (Eq. (9)), as well as the isn complex, offer the advantage of providing a strong bond between the ruthenium complex and the matrix, thus preventing leaching of the complex during manipulations.

The same procedure described for K[Ru(Cl)(Hedta)] immobilization has been applied for homogeneous matrices, such as the PAMAM dendrimers with terminal amine groups. Due to their structural properties and multivalent surface, large quantities of

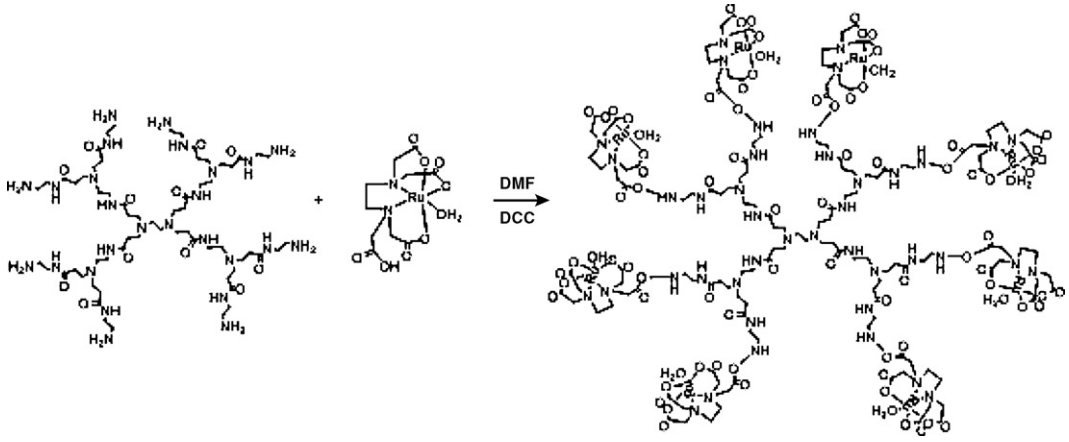

Scheme 3. Schematic representation for the preparation of immobilized K[Ru(Cl)(Hedta)] on the PAMAM dendrimer.

$$Na\text{-}Y + [Ru(NH_3)_4LL']^{2+/3+} \xrightarrow[solvent]{Ar(g)} Na^+ + [Ru(NH_3)_4LL']\text{-}Y$$

Where: L = SO_2, NH_3, H_2O and L'= NH_3, H_2O, dtdp or pz

Scheme 4. Encapsulation of ruthenium ammines in Na-Y zeolite. Where: L = SO_2, NH_3, H_2O and L′ = NH_3, H_2O, dtdp or pz.

a desired species can be stored by a single dendrimer molecule, thereby making them particularly attractive as drug carriers. The attachment of this species on PAMAM dendrimers may be useful for enhancing the retention time of the desired species in the bloodstream.

The reaction below (Scheme 3) has been studied using different generations of PAMAM, with terminal amine groups being easily converted to amide via reaction with the unbound carboxylic moiety present in the edta ligand [6].

2.2. Zeolite

Metal complexes can be immobilized inside zeolite cavities by direct ionic exchange reactions between the zeolite and the ion complex followed by ligand coordination or not [76–79]. Specifically, $[Ru(NH_3)_6]Cl_3$, *cis*-$[Ru(H_2O)_2(NH_3)_4](PF_6)_2$, *trans*-$[Ru(H_2O)(NH_3)_4(SO_2)](tfms)_2$, *trans*-$[Ru(NH_3)_5(dtdp)](PF_6)_2$, and *trans*-$[Ru(NH_3)_5(pz)](PF_6)_2$ complexes have been encapsulated into Na-Y zeolite, according to Scheme 4.

2.3. Entrapped ruthenium complexes

Materials obtained by the sol–gel process may display desired properties such as optical transparency and chemical and mechanical stability [33]. Also, they can be prepared in different sizes and shapes, including thin films, monoliths, membranes and powders [33,80–82]. In addition, the mild conditions used in this process make it suitable for the immobilization of such different species as dyes [83], metal complexes [18,21,32] and even proteins [84,85]. Compared with silica gel, this method may allow for a larger load of complex since the entrapment is not limited by the density of functional groups, as in the case of the silica surface. Unlike silica materials, not all the complexes are readily available in the

xerogel because they are entangled in the bulk of the material. From this point of view, studies carried out in our Laboratories resulted in the entrapment of *trans*-[Ru(NO)Cl(cyclam)]$(PF_6)_2$ [21], and [Ru(NO)(salen)(H_2O)](NO_3), [32] which are based on silane or silane/organosilane xerogel materials. These nitrosyl complexes were entrapped with loads of complexes lower than those reported in the case of the silica gel support, despite a much larger load is possible.

Besides these materials, the incorporation of [Ru(terpy)(L)(NO)]$(PF_6)_3$ (L = bpy and NH.NHq) complexes [28], *cis*-[Ru(NO_2)(bpy)$_2$(4-pic)](PF_6) and a macrocyclic complex named *trans*-[RuCl([15]aneN$_4$)(NO)]$(PF_6)_2$ ([15]aneN$_4$ = 1,4,8,12-tetraazacyclopentadecane) into silicone membranes have been also studied. The silicone membrane is a composite obtained by a non-hydrolytic sol–gel route using TEOS and PDMS (polydimethylsiloxane). The macrocyclic *trans*-[RuCl([15]aneN$_4$)(NO)]$(PF_6)_2$ complex, free or incorporated in silicone membrane with [Ru$(NH_3)_5$(pz)]$(PF_6)_2$ as photosensitizer, was also studied as a nitric oxide photo-release agent [86]. Basically, the silicone resin was prepared by mixing PDMS, TEOS and di-n-butyltindilaurate in isopropylic alcohol. The nitrosyl complex [Ru(terpy)(L)(NO)]$(PF_6)_3$, *cis*-[Ru(NO_2)(bpy)$_2$(4-pic)](PF_6), or *trans*-[RuCl([15]aneN$_4$)(NO)]$(PF_6)_2$ was added to this mixture and air-dried at room temperature, for 24 h.

The amount of NO available per volume of the matrix can be controlled by the amount of nitrosyl ruthenium complex, which can be convenient for tissue exposure to such materials, since the tissue can be provided with different NO dosages.

2.3.1. Encapsulation in biodegradable polymeric micro or nanoparticles

Some of the most widely used polymers for micro or nanoparticles preparation are PLA, PGA, and their co-polymer, PLGA [14,87–99]. Two methods are commonly used for encapsulation of compounds in micro or nanoparticles, depending on the hydrophilic nature of the drug to be entrapped. Hydrophobic compounds are entrapped by a single emulsion process that involves oil-in-water (o/w) emulsification. The organic volatile solution of polymer and drug is emulsified in a larger volume of water, with appropriate stirring and temperature conditions, in the presence of an emulsifying agent, like poly(vinyl alcohol), to yield an o/w emulsion. Solid microparticles are obtained after solvent removal and evaporation, washed, and collected by centrifugation [14,89,90]. One of the disadvantages of the o/w emulsification method is the poor encapsulation efficiency of moderately water-soluble and water-soluble drugs [14,88]. The compound would diffuse out or partition from the dispersed oil phase into the aqueous continuous phase, and microcrystalline fragments of the hydrophilic compounds would get deposited on the microparticle surface and dispersed in the PLGA matrix [91–93]. This would result in poor trapping of a hydrophilic drug, such as *trans*-[Ru(NO)$(NH_3)_4$(py)]$(BF_4)_3$ [14], and initial rapid release of the compound (burst effect) [94,95]. The double (multiple) emulsion process, which is a water-in-oil-in-water (w/o/w) method, is best suited for encapsulation of water-soluble compounds, such as peptides, proteins, and vaccines, unlike the o/w method, which is ideal for water-insoluble drugs, like steroids [91–93,96–98].

A double emulsion technique consists in dissolving the drug in distilled water or in a buffer solution (inner water phase) while the polymer is dissolved in a volatile organic solvent that is not miscible with water (organic phase). The inner water phase (containing a surfactant or not) is then poured into the organic phase. This mixture is generally emulsified forming the first inner emulsion or the primary emulsion (w/o). This w/o emulsion is then poured under vigorous mechanical stirring into an aqueous phase (outer water phase) that contains an emulsifier, thus forming the double w/o/w emulsion. The resulting multiple emulsion is continuously stirred and the solvent is allowed to evaporate, thereby inducing polymer precipitation and formation of solid drug-loaded microspheres [14,95]. Among these methods for nano/microparticle preparation, the most suitable one for immobilization of water-soluble ruthenium complexes is the double emulsion method [95].

Nano and microparticles have become an important area of research in the field of drug delivery because they are able to deliver a wide range of drugs to different areas of the body for sustained periods of time. The small size of the microparticles is of utmost importance for systemic circulation [47,99].

2.3.2. Silicone and hydrogel

[Ru(NO)(terpy)(L)]$(PF_6)_3$, L = bpy or NH.NHq complexes, *cis*-[Ru(NO_2)(bpy)$_2$(4-pic)](PF_6), and *trans*-[RuCl([15]aneN$_4$)(NO)]-$(PF_6)_2$, have been entrapped into a silicone membrane and a hydrogel, which are currently used for topical administration of drugs [100,101]. The polymers chosen to form the gels have different ionic characteristics (non-ionic, cationic, and anionic hydrogels) to allow for evaluation of the interactions established by the positively charged nitro-donor complex and the vehicles. In order to prepare a non-ionic, an anionic, and a cationic hydrogel, three different gel-forming polymers, namely HEC, Carbopol, and Chitosan, were respectively dispersed into appropriate amounts of an aqueous solution saturated with *cis*-[Ru(NO_2)(bpy)$_2$(4-pic)](PF_6) [102]. Chemical crosslinked chitosan gels containing three different glutaraldehyde (GLU) concentrations (0.01%, 0.03%, and 0.05%) were also obtained.

3. Characterization and reactivity of solution and immobilized species

3.1. EPR Spectroscopy

Table 1 lists EPR data for some non-immobilized and immobilized ruthenium complexes. From the *g* values and linewidth parameters it is possible to infer that immobilization of metal complexes in the matrices (modified silica gel, Na-Y zeolite) promotes distortions in the structure and symmetry of the complexes. A decrease in the linewidth is observed when the complexes are immobilized into/onto the matrices. This would be consequence of the stiffening and the higher separation of the immobilized molecules, which should diminish the interaction between the complexes [104].

All complexes listed in Table 1 exhibit strong field d^5 Ru(III) configuration. In this case the value of *g* tensor depends on the energy and the configuration of the t_2 bonding orbitals [71,105]. The parameters used to calculate the energy of the t_2 orbitals: V (defined as $V = E(d_{xz}) - E(d_{yz})$) and Δ (defined as $\Delta = E(d_{xy}) - 0.5[E(d_{xz}) - E(d_{yz})]$) [106] are qualitatively defined by the *g* values. For all the complexes listed in Table 1, $g_{\|} < g_{\perp}$ implicating that the value of $V = 0$, and consequently the value of Δ, assumes a positive value. Thus, two of the t_2 orbitals are degenerate (d_{xz} and d_{yz}), while the third one has higher energy (d_{yz}) [107].

The presence of two distinct *g* values are consistent with a C_{4v} and C_{2v} (for the *cis* complexes) point group symmetry for all the complexes listed in Table 1, except for the [Ru$(NH_3)_6$]Cl_3 complex, which exhibits only one *g* value (*g* iso = 1.97), coherent with the O_h point group symmetry. When [Ru$(NH_3)_6$]Cl_3 is immobilized in Na-Y zeolite, two different *g* values can be observed ($g_{\perp} = 2.14$ and $g_{\|} = 1.78$) [78], which is compatible with a tetragonal distortion of the structure [79]. Comparing the spectrum of the [Ru$(NH_3)_6$]Cl_3 complex and that of the occluded [Ru$(NH_3)_6$]–Y (Fig. 1), there are noticeable differences between the two species in terms of linewidth as depicted in Table 1. A careful examination of

Table 1
g and linewidht values for selected non-immobilized/immobilized ruthenium complexes.

Compound	g_{iso}	$g_{\perp}$	$g_{\|\|}$	Lw (Gauss)	Ref.
[≡Si(CH$_2$)$_3$(im*N*)Ru(SO$_4$)(NH$_3$)$_4$]Cl[(a)]		2.39	2.31	410	[103]
trans-[Ru(NH$_3$)$_4$(SO$_4$)(im*N*)]BF$_4$[(b)]		2.46	1.40	500	[71]
trans-[Ru(NH$_3$)$_4$(SO$_4$)(pz)]BF$_4$[(b)]		2.40		(*)	[71]
[(4-PVP)Ru(SO$_4$)(NH$_3$)$_4$]Cl[(b)]		2.31		430	[19]
[(4-PVP)Ru(H$_2$O)(NH$_3$)$_4$]Cl$_3$[(b)]		2.00		425	[19]
[Ru(NH$_3$)$_6$]Cl$_3$–Y[(a)]		2.14	1.78	368	[78,79]
[Ru(NH$_3$)$_6$]Cl$_3$[(b)]	1.97			868	[78,79]
cis-[Ru(H$_2$O)$_2$(NH$_3$)$_4$](tfms)$_3$–Y[(b)]		2.21	1.57	120	[76–79]
cis-[Ru(H$_2$O)$_2$(NH$_3$)$_4$](tfms)$_3$[(b)]		2.13	1.26	242	[76–79]

Lw: linewidth; *g* iso: isotropic *g* value; $g_{\perp} = g_x + g_y$: perpendicular *g* value; $g_{||} = g_z$: parallel *g* value; []–Y: occluded in the Na-Y zeolite; (a) $T = 4$ K; (b) $T = 77$ K; (*) line too broad to be measured.

the spectrum (Fig. 1B) reveals a small hyperfine splitting, probably caused by the interaction of the oxygen atoms of the zeolite structure (AlO_4^-) with the ammonia ligand of [Ru(NH$_3$)$_6$]Cl$_3$ (Fig. 1). This interaction would cause the delocalization of the unpaired electron of the Ru(III) center to the nitrogen, explaining the observed hyperfine splitting. Changes in *g* values are also observed in the spectrum of *cis*-[Ru(H$_2$O)$_2$(NH$_3$)$_4$](tfms)$_3$ located in the zeolite Na-Y cavity, which follows the same pattern of [Ru(NH$_3$)$_6$]Cl$_3$. The small signal around 2250 Gauss in the Fig. 1B is relative to Fe(III) impurities in the zeolite cage.

The spectrum of the complex with pyrazine, *trans*-[Ru(SO$_4$)(NH$_3$)$_4$(pz)]BF$_4$, shows just the $g_{\perp}$ value, since the measurement of the line relative to $g_{||}$ is virtually impossible due to the line broadness [73,106], which makes its precise determination very difficult. Indicative of reaction, immobilization of this complex in 4-PVP results in changes in the $g_{\perp}$ value. However, as in the previous case, no clear signal corresponding to $g_{||}$ appears in the EPR spectrum. The same behavior is also observed for the corresponding aquo species.

The matrix effect could also be observed in the EPR spectrum of the frozen [Ru(edta)(H$_2$O)]$^{2+}$ solution. The spectrum of the non-immobilized [Ru(edta)(H$_2$O)]$^{2+}$ could not be detected even at liquid helium temperature (4 K), since the spin-lattice relaxation is very short, thereby resulting in a noised and broad band signal spectrum [108]. However, when immobilized in PAMAM-type dendrimers (generation 0, 2, and 3), this complex exhibits quite a different spectrum. At liquid nitrogen temperature (77 K) it is possible to record a spectrum because the complex immobilization into a rigid matrix makes the spin-lattice relaxation longer enough to be detected [6].

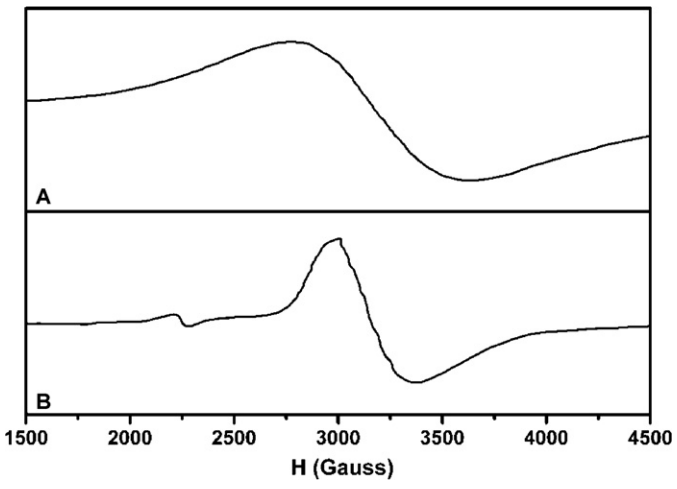

Fig. 1. EPR powder spectra of the complex [Ru(NH$_3$)$_6$]Cl$_3$ (A): non-occluded; (B): occluded in Na-Y zeolite. $T = 77$ K; Microwave Frequency = 9.4 GHz.

The results discussed above indicate that EPR spectroscopy is quite useful to characterize reactions of the ruthenium metal complex with the supra-cited matrices in two ways: determination of the oxidation state of the metal center of the immobilized/bonded complex and the distortions in the point group symmetry of the molecules when they are immobilized in the matrices.

3.2. Vibrational spectroscopy

Table 2 lists some IR spectroscopic data for several immobilized and non-immobilized complexes and related species.

The IR characterization of silica gel based matrices is complicated, since the starting material absorbs strongly at 1630 cm^{-1} (water) and below 1300 cm^{-1}, making the definition of bands in this region impossible. Silica gel has weak IR absorptions in the region between 2800 and 1650 cm^{-1} [4,29], but they are strong enough to allow the characterization of the immobilized complexes (Table 2). Nevertheless, IR spectroscopy is useful to detect immobilized ruthenium complexes with strong π-acid ligands such as CO, CN$^-$, and NO. When coordinated to the metal center, these ligands exhibit characteristic intense bands in the region between 2200 and 1850 cm^{-1} [115]. In all the listed matrices, the anchoring reaction leads to a red shift around 50 cm^{-1} in the bands relative to ν(CO) and ν(CN$^-$) [4,103]. In this case, the interpretation is not so straightforward since the matrix effect would overlap with eventual changes in the back-bonding between the $Ru_{d\pi}$ and p_{π^*} orbitals of the ligands. A different behavior was noticed for immobilized/non-immobilized nitrosyl complexes, for which no significant shift of the ν(NO) band was observed [7,20]. For the TiO$_2$/silica based matrix, the same inconvenient silica absorption occurs [110]. As an example of the modified silica anchored complexes, the strong ν(CN$^-$) band could be identified, being indicative of the reaction between the complex and the TiO$_2$/Silica gel matrix [5].

Since xerogel based materials consist essentially of a silica network, there are the same complications in their IR spectra as those observed for silica gel. The ν(NO) band in the diffuse reflectance IR spectrum of *trans*-[Ru(NO)Cl(cyclam)](PF$_6$)$_2$ entrapped in the SiO$_2$ matrix appears at 1870 cm^{-1}, similar to those observed for organosilane with n-propyl (SiPr) or mercaptopropyl (SiSH) hybrid materials (SiO$_2$/SiSH and SiO$_2$/SiPr), which are located at 1875 cm^{-1}. These values are essentially the same observed for *trans*-[Ru(NO)Cl(cyclam)](PF$_6$)$_2$ (1875 cm^{-1}). For the SiO$_2$/SiNH$_2$ material ν(NO) is shifted to 1854 cm^{-1}, as a result of the nucleophilic attack of the amino group of 3-aminopropyltriethoxysilane to *trans*-[Ru(NO)Cl(cyclam)](PF$_6$)$_2$ [21,112]. On the other hand, contrasting with the behavior of functionalized silica matrices, the [Ru(NO)(H$_2$O)(salen)](NO$_3$) xerogel ν(NO) is shifted 20 cm^{-1} from that of [Ru(NO)(salen)(H$_2$O)](NO$_3$) (1836 cm^{-1}) [32].

Table 2
Some infrared data for immobilized/non-immobilized ruthenium complexes.

Compound	Wavenumber (cm^{-1})		Attribution	Ref.
Silica gel	1875	w	silica skeleton	[29,109]
	1630	s	δ(H-O-H) water	
	>1300	s	silica skeleton	
≡Si(CH_2)$_3$(im*N*)	1580	m	ν(C-C)/ν(C-H) im*N* ring	[4]
	1548	m	ν(C-C) im*N* ring	
	1450	s	ν(C-N) im*N* ring	
	1408	s	δ(CH_2)	
[≡Si(CH_2)$_3$(im*N*)Ru(NH_3)$_4$(L)]Cl_2	1560	m	ν(≡Si(CH_2)$_3$(im*N*))	[3,103]
(L = SO_2; SO_4^{2-}; H_2O)	1515	m	δ(C-C) im*N* ring	
	1550	w	ν(C-N) pz ring	
[≡Si(CH_2)$_3$(im*N*)Ru(C_2O_4)(NH_3)$_4$]Cl_2	1698	m	ν(C=O)	[3]
[≡Si(CH_2)$_3$(im*N*)Ru(CN)(NH_3)$_4$]Cl_2	2040	m	ν(CN)	[3]
[≡Si(CH_2)$_3$(im*N*)Ru(CO)(NH_3)$_4$]Cl_2	1938	s	ν(CO)	[3]
[≡Si(CH_2)$_3$(im*N*)Ru(NO)(NH_3)$_4$]Cl_3	1919	s	ν(NO)	[3]
≡Si(CH_2)$_3$(dpp)	1555	w	ν(N-H) NH_2	[3]
[≡Si(CH_2)$_3$(dpp)Ru(CN)(NH_3)$_4$]Cl	2088	m	ν(CN)	[3]
[≡Si(CH_2)$_3$(dpp)Ru(CO)(NH_3)$_4$]Cl_2	1987	m	ν(CO)	[3]
K_4[≡SiTi(O)Ru(CN)$_6$]	2058	s	ν(CN)	[110]
≡Si(CH_2)$_3$(isn)	1554	m	ν(CO)	[20]
[≡Si(CH_2)$_3$(isn)Ru(NO)(NH_3)$_4$](PF_6)$_3$	1930	s	ν(NO)	[20]
trans-[Ru(NO)(NH_3)$_4$(isn)](BF_4)$_3$	1928	s	ν(NO)	[111]
SiO_2/*trans*-[Ru(NO)Cl(cyclam)](PF_6)$_2$	1870	s	ν(NO)	[21]
SiO_2/SiSH/*trans*-[Ru(NO)Cl(cyclam)](PF_6)$_2$	1875	s	ν(NO)	[112]
SiO_2/$SiNH_2$/*trans*-[Ru(NO)Cl(cyclam)](PF_6)$_2$	1854	s	ν(NO)	[21]
SiO_2/SiPr/*trans*-[Ru(NO)Cl(cyclam)](PF_6)$_2$	1875	s	ν(NO)	[112]
trans-[Ru(NO)Cl(cyclam)](PF_6)$_2$	1875	s	ν(NO)	[57]
SiO_2/[Ru(NO)(OH_2)(salen)](NO_3)	1856	s	ν(NO)	[32]
[Ru(NO)(salen)(H_2O)](NO_3)	1836	s	ν(NO)	[32]
4-PVP	1599	s	ν(C-N) py ring	[19]
	1414	s	ν(C-C) py ring	
[(4-PVP)Ru(NH_3)$_4$(SO_2)]Cl	1673	m	ν(C-N) py ring	[19]
	1557	s	ν(C-N) py ring	
	1276	s	ν(SO_2) asym.	
	1260	s	ν(SO_2) asym.	
	1200	w	ν(SO_2) asym.	
	1030	s	δ(SO_2)	
[(4-PVP)Ru(CN)(NH_3)$_4$]Cl	2044	m	ν(CN)	[3]
trans-[Ru(H_2O)(NH_3)$_4$(SO_2)](tfms)$_2$	1631	w	δ(NH_3)(a)	[72]
	1287	s	ν(SO_2) asym.	
	1255	s	ν(SO_2) asym.	
	1177	s	ν(SO_2) asym.	
	1034	s	δ(SO_2)	
trans-[Ru(H_2O)(NH_3)$_4$(im*N*)](PF_6)$_2$	1630	s	δ(NH_3)(a)	[72]
	1561	m	ν(C-C) im*N* ring	
	1440	s	ν(C-N) im*N* ring	
	1535	m	δ(N-H)	
	1473	w	δ(C-H)	
	1414	m	ν(C-N)	
	1391	s	δ(C-H)	
trans-[Ru(CN)(NH_3)$_4$(im*N*)]PF_6	2076	s	ν(CN)	[3]
HCN(g)	2091	s	ν(CN)	[113]
trans-[Ru(CO)(NH_3)$_4$(im*N*)](PF_6)$_2$	1985	s	ν(CO)	[3]
$CO_{(g)}$	2155	s	ν(CO)	[113]
trans-[Ru(NO)(NH_3)$_4$(im*N*)](PF_6)$_3$	1920	s	ν(NO)	[58]
trans-[Ru(CN)(NH_3)$_4$(dpp)](PF_6)$_2$	2071	s	ν(CN)	[114]
trans-[Ru(CO)(NH_3)$_4$(dpp)](PF_6)$_2$	1995	s	ν(CO)	[114]
K_4[Ru(CN)$_6$]	2048	s	ν(CN)	[115]
Na-Y	1640	s	δ(H_2O) sym	[78]
	3460	s	ν(H_2O)	[78]
[Ru(NH_3)$_6$]Cl_3–Y	1652	s	δ(NH_3) asym	[78]
cis-[Ru(H_2O)$_2$(NH_3)$_4$](tfms)$_3$–Y	1680	s	δ(H_2O) sym	[76–79]
	1616	sh	δ(NH_3) asym	
	1321	w	δ(NH_3) sym	
trans-[Ru(H_2O)(NH_3)$_4$(SO_2)](tfms)$_2$–Y	1661	sh	δ(H_2O) sym	[76–79]
	1639	s	δ(NH_3) asym	
	1319	sh	δ(NH_3) sym	
trans-[Ru(H_2O)(NH_3)$_4$(P(OEt)$_3$)](tfms)$_3$–Y	1646	s	δ(H_2O) sym	[76–79]
[Ru(NH_3)$_5$(pz)]–Y	1646	s	δ(H_2O) sym	[76–79]

Table 2 (*Continued*)

Compound	Wavenumber (cm^{-1})		Attribution	Ref.
$[Ru(NH_3)_5(dtdp)]$–Y	1640	s	$\delta(H_2O)$ sym	[76–79]
	1324	sh	$\delta(NH_3)$ sym	
	1312	sh	$\delta(NH_3)$ sym	
	1226	sh	δ(C-H)	
	1633	sh	$\delta(NH_3)$ asym	
	1397	w	ν(C-CH_2) asym	
$[Ru(NH_3)_6]Cl_3$	1607	s	$\delta(H_2O)$ sym	[78]
	1319	s	$\delta(NH_3)$ sym	
cis-$[Ru(H_2O)(NH_3)_4(SO_2)](tfms)_3$	1635	m	$\delta(NH_3)$ asym	[3]
	1326	sh	$\delta(NH_3)$ sym	
	1264	w	$\delta(NH_3)$ sym	
$[Ru(NH_3)_5(pz)](PF_6)_2$	1631	s	$\delta(NH_3)$ asym	[76–79]
	1584	s	ν(C-C)	
	1341	sh	$\delta(NH_3)$ sym	
	1292	s	δ(C-H)	
$[Ru(NH_3)_5(dtdp)](PF_6)_2$	1626	s	$\delta(NH_3)$ asym	[3]
	1584	m	ν(C-C)	
	1484	m	ν(C-C)	
	1414	w	ν(C-C)	
	1384	sh	ν(C-C)	
	1285	m	$\delta(NH_3)$ sym	
PAMAM-G_x	3285	s	ν(N-H)	[116]
	2944	s	ν(C-H)/ν(C-N)	
	2845	s	ν(C-H)	
	1642	m	ν(C=O)	
	1550	w	ν(C-N)/ν(N-H)	
	1465	w	$\delta(CH_2$-N)	
	1436	w	$\nu(COO^-)$ sym	
	1245	w	$\nu(COO^-)$ sym	
G_x[RuCl(Hedta)]	2940	s	ν(C-H)/ν(C-N)	[6]
	2861	s	ν(C-H)	
	1732	m	$\nu(COO^-)$ asym	
	1649	m	ν(C=O) asym	
	1284	w	$\nu(COO^-)$ asym	
G_x[Ru(NO)(Hedta)]	1890	s	ν(NO)	[6]
K[RuCl(Hedta)]	1728	m	$\nu(COO^-)$ asym	[6,7]
	1426	w	$\nu(COO^-)$ sym	
[Ru(NO)(Hedta)]	1890	s	ν(NO)	[6]
	1264	w	$\nu(COO^-)$ sym	

s: strong; m: medium; w: weak; sh: shoulder; (a) equatorial NH_3; sym: symmetric; asym: asymmetric.

The IR spectrum of 4-PVP is relatively clear in 2500–800 cm^{-1} [19] region with only two strong bands at 1599 and 1414 cm^{-1}, attributed to the pyridine ring. This allows the detection of coordinated SO_2, whose bands lie in the 1200–1000 cm^{-1} range [115] before and after immobilization. A matrix effect in this case is also observed, since the bands of the non-immobilized complexes are red-shifted when they are anchored in the 4-PVP. The shifts in the stretching frequencies for the SO_2 ligand in immobilized/non-immobilized *trans*-$[Ru(H_2O)(NH_3)_4(SO_2)](tfms)_2$ can be observed in Table 2.

The zeolite Na-Y is transparent in the 3000–1650 cm^{-1} IR region [78,79]. Water adsorbed in the zeolite has two strong absorptions around 1640 and 3500 cm^{-1}. The principal evidence of complex occlusion is the presence of the band relative to the symmetric angular deformation of the coordinated NH_3 ligands (around 1300 cm^{-1}), absent in the support [78]. Interaction of the complexes with the matrix shifts their bands, particularly the bands relative to $\delta(H_2O)$ of the zeolite and $\delta(NH_3)$ of the equatorial ammonias of the ruthenium complexes [78]. Generally, this shift is to higher wavenumbers, indicating that the interaction between the complex and the zeolite change the dipoles of the matrix.

PAMAM dendrimers also absorb strongly in the IR regions between 3300 and 2800 cm^{-1} and 1650–1250 cm^{-1} [116]. However, the region between 2800 and 1650 cm^{-1} is clear and allows identification of the stretching frequencies of ligands such as CN^-, CO, and NO. The principal change in the IR spectra of the immobilized/non-anchored K[Ru(Cl)(Hedta)] is the increase in the absorption in the region of 1700 cm^{-1}, attributed to the presence of the carboxyl and amide groups of the Hedta [117]. For the anchored [Ru(NO)(Hedta)], the band relative to ν(NO) (1890 cm^{-1}) was used to confirm the anchoring [6].

The characteristic NO band (1928 cm^{-1}) for *trans*-$[Ru(NO)(NH_3)_4(py)](BF_4)_3$ seems to be enveloped when the complex is loaded into PLGA microparticles, because of the very strong and broad carbonyl band (1761 cm^{-1}) from the PLGA polymer, which renders this technique not so convenient in this case. This result is attributed to the relatively high concentration of PLGA in the microparticle [14].

3.3. UV–vis spectroscopy

Table 3 summarizes the UV–vis results for the non-immobilized and immobilized complexes in a range of matrices. In most of

the complexes summarized in Table 3, the charge-transfer bands involve the Ru $4_{d\pi}$ and ligands π^* orbitals [118,119]. These tentative attributions were made by comparing the spectra of the non-immobilized complexes with those of the immobilized ones.

The immobilization of the ruthenium complexes into/onto the solid matrices renders the complex insoluble. For this reason, the electronic spectroscopic measurements were carried out in chloroform or carbon tetrachloride suspension, since their refraction index is similar to that of silica gel [4]. Diffuse reflectance with the samples dispersed in MgO or photoacoustic spectroscopy was used as an alternative to the suspension method for some immobilized complexes. These techniques introduce experimental inconveniences. By using a chloroform or carbon tetrachloride suspension, the light scattering caused by the particles in suspension leads to a broadening of the band [4]. The particle size of MgO used for making the dispersion of the analyte in diffuse reflectance spectra also causes broadening similar to the one observed in the chloroform suspension spectrum [4]. For example, comparing the charge-transfer band width at half of its height for the non-immobilized and silica-immobilized *trans*-$[Ru(CO)(NH_3)_4(imN)](PF_6)_2$, it is possible to observe a broadening of 750 cm^{-1} in the band of the spectrum obtained using diffuse reflectance regarding the measurement for the complex in aqueous solution. Due to the intrinsic limitation of the dispersion techniques, molar absorptivity data were not reported. Thus, for the complexes listed in Table 3, the shifts in the charge-transfer bands were mainly used for comparison of the behaviors of the non-immobilized and immobilized complexes. The use of 4-PVP or PAMAM dendrimers as a matrix leads to non-significant shifts in the bands [3,6]. The bands found in the diffuse reflectance or photoacoustic spectra were attributed by comparison with the ones described for the corresponding complexes in solution.

By analyzing the spectra of non-supported/supported ruthenium complexes in silica gel functionalized with $\equiv Si(CH_2)_3(L)$ (im*N* or isn), it is possible to observe that anchoring of the complex in the matrix does not lead to significant changes in the MCLT band energies. The band relative to the d → d transition is not detected since this transition is probably enveloped by the charge-transfer band [4,20]. For the ruthenium tetraammine complexes immobilized in $\equiv Si(CH_2)_3$(isn) silica gel, two absorption bands are observed. One is in the 268–274 nm region and is probably due to isonicotinamide internal ligand (IL) transitions, since the free ligand and $\equiv Si(CH_2)_3$(isn) show a band in this region. For the Ru(II)-immobilized complexes containing SO_3^{2-}, SO_2, and H_2O ligands, a second absorption band is seen in the 380–492 nm range. These bands have been attributed [74,126–128] to MLCT Ru(II) → L (L = N heterocyclic) transitions. The immobilized nitrosyl ruthenium ammine shows one absorption band at λ = 330 nm, which is similar to the one observed for this complex in solution. The other absorption bands are not detected in the UV–vis spectra. This is probably due to matrix absorption, which masks the band at 230 nm and the very low molar absorption band at 486 nm ($\varepsilon = 4.4 \times 10^1\ M^{-1}\ cm^{-1}$) observed for the complex in solution [20,63]. One absorption is defined at 340 nm for the Ru(III) species, $[\equiv Si(CH_2)_3(isn)Ru(SO_4)(NH_3)_4]Cl_3$, which has been attributed to a ligand–metal charge transfer (LMCT) [71,73]. Although some shifts are observed for the immobilized complexes, the maximum absorption band values are in agreement with those observed for the complexes in solution.

A clear shift in energy is observed for immobilized *trans*-$[Ru(NH_3)_4(imN)(pz)](PF_6)_2$. As shown in Table 3, anchoring of the complex in the support leads to a blue shift (15 nm) in the MLCT band due to Ru → pz, and a red shift (12 nm) in the Ru → im*N* MLCT band regarding to the spectrum of the non-anchored complex. This would be consistent with the weakening of the intensity of the back-bonding Ru → im*N* and strengthening of the back-bonding Ru → pz. For the other ruthenium tetrammines anchored in modified silica gel, the shift of the bands is smaller than the reported values and does not allow the same interpretation.

The electronic spectra of ruthenium nitrosyls *trans*-$[Ru(NO)Cl(cyclam)](PF_6)_2$ and $[Ru(NO)(H_2O)(salen)](NO_3)$ entrapped in xerogel matrices, obtained in CCl_4 suspension, showed some differences regarding the analogous species in solution. The *trans*-$[Ru(NO)Cl(cyclam)](PF_6)_2$ complex in solution displays bands centered around 265, 350, and 430 nm [57,129]. The low energy band ($\varepsilon = 54\ cm^{-1}\ M^{-1}$) is barely seen after entrapment into the xerogel, probably due to its low intensity and the light scattering of the solid. A more significant difference is observed in the UV–vis spectra of this complex entrapped in $SiO_2/SiNH_2$. This material shows a band at 484 nm, which is attributed to the product formed from the nucleophilic attack of the 3-aminopropyltriethoxysilane NH_2 to *trans*-$[Ru(NO)Cl(cyclam)](PF_6)_2$ [21].

For the silica modified with TiO_2 the UV–vis spectrum is more enlightening, as shown in Table 3. The MLCT band attributed to the $Ru_{4d\pi}$ to the p_{π^*} CN^- orbitals in the $K_4[Ru(CN)_6]$ complex is red-shifted by 158 nm upon anchoring onto the titanium surface [31,123]. The hetero binuclear complex in solution $[(CN)_5Ru(CN)Ru(NH_3)_5]Cl$ exhibits a MMCT band centered at 680 nm, and a strong absorption below 300 nm is tentatively attributed to the hexacyano moiety [124]. When this complex is anchored, the two bands reported for the non-anchored complex are red-shifted to 369 nm (MLCT) and 642 nm (MMCT). In solution and in the presence of Zn^{2+}, there is formation of the $Zn[\equiv SiTiO(CN)_5Ru(CN)Ru(NH_3)_5]$ species, with bands at 366 and 580 nm, attributed to MLCT and MMCT transitions, respectively. These bands are red-shifted regarding the ones observed for the $Zn[(CN)_5Ru(CN)Ru(NH_3)_5]_2$ complex (Table 3). For all the complexes anchored in modified silica with titanium, the red shift is attributed to the stabilization of the HOMO orbitals of the complexes due to the interaction with the titanium ion, dispersed in the silica gel surface [123].

The interaction of the complexes with the negatively charged zeolite cage also induces changes in the UV–vis spectrum. For the $[Ru(NH_3)_6]Cl_3$ complex, the LMCT band at 275 nm undergoes a small but noticeable and reproducible blue shift to 270 nm [78]. The ligand-field transition for the non-immobilized complex at 323 nm is not observed for the immobilized complex since it is probably enveloped by the more intense LMCT band. For the *trans*-$[Ru(H_2O)(NH_3)_4(SO_2)](tfms)_2$ complex, the position of the bands is pH dependent, since the ligand SO_2 shows $SO_2/HSO_3^-/SO_3^{2-}$ acid–base equilibria. At pH < 2.0, the complex is mostly in the SO_2 form in solution; when pH > 5.5, the SO_3^{2-} species predominates [72,118]. This is confirmed by the pK_a measurements for the occluded and non-occluded complexes carried out by electrochemical methods [3,103]. In both cases, a red shift (20 nm) of the LMCT bands is observed. This would suggest interaction of the SO_2/SO_3^{3-} groups with the charged zeolite cage, inducing changes in the charge-transfer process. The same red shift in the MLCT bands is observed for the *trans*-$[Ru(NH_3)_5(dtdp)](PF_6)_2$ complex. For *cis*-$[Ru(H_2O)_2(NH_3)_4](tfms)_3$, the band at 253 nm, attributed to the LMCT process, is not identified in the case of the occluded complex. The occluded $[Ru(NH_3)_5(pz)]Cl_2$ has a different behavior from the other occluded complexes. Its MLCT band is blue shifted and the appearance of a new band with $\lambda_{max} = 580$ nm is observed. A clear interpretation for that is still needed. However, as observed from EPR measurements, the $[Ru(NH_3)_6]Cl_3$ symmetry distortions are clearly observed when the complex is entrapped into the zeolite. Furthermore some interaction between the non-protonated nitrogen atom of the pyrazine ligand (pK_a around 2.5) [125] with the

Table 3
Electronic spectroscopy data[1] and formal reduction potentials (E_f') for non-immobilized/immobilized ruthenium complexes.

Compound	λ_{max}[2] (nm)	E_f' V vs. NHE[3]	Ref.
[≡Si(CH$_2$)$_3$(im*N*)Ru(H$_2$O)(NH$_3$)$_4$]Cl$_2$	350 [a] 440 [d]	0.03	[4]
trans-[Ru(H$_2$O)(NH$_3$)$_4$(im*N*)](PF$_6$)$_2$	326 [a]	0.10	[118,119]
[≡Si(CH$_2$)$_3$(im*N*)Ru(NH$_3$)$_4$(isn)]Cl$_2$	337 [a] 426 [b] 435 [b][4]		[4]
trans-[Ru(NH$_3$)$_4$(im*N*)(isn)]Cl$_2$	342 [a] 430 [b]		[118–120]
[≡Si(CH$_2$)$_3$(im*N*)Ru(CN)(NH$_3$)$_4$]Cl	350 [a] 329 [b] 317 [b][4]		[4]
trans-[Ru(CN)(NH$_3$)$_4$(im*N*)](PF$_6$)$_2$	344 [a] 324 [b]		[4]
[≡Si(CH$_2$)$_3$(im*N*)Ru(NH$_3$)$_4$(pz)]Cl$_2$	329 [a] 439 [b] 455 [b][4]	0.46	[4]
trans-[Ru(NH$_3$)$_4$(im*N*)(pz)](PF$_6$)$_2$	345 [a] 448 [b]	0.49	[118–120]
[≡Si(CH$_2$)$_3$(im*N*)Ru(CO)(NH$_3$)$_4$]Cl$_2$	345 [a] 301 [b] 294 [b][4]		[4]
trans-[Ru(CO)(NH$_3$)$_4$(im*N*)](PF$_6$)$_2$	340 [a] 297 [b]		[4]
[≡Si(CH$_2$)$_3$(im*N*)Ru(C$_2$O$_4$)(NH$_3$)$_4$]Cl	351 [a] 297 [b] 294 [b]		[4]
trans-[Ru(C$_2$O$_4$)(NH$_3$)$_4$(im*N*)]Cl$_2$	349 [a] 302 [b]		[4]
[≡Si(CH$_2$)$_3$(im*N*)Ru(NH$_3$)$_4$(SO$_2$)]Cl$_2$	340 [a]	0.33	[103]
[≡Si(CH$_2$)$_3$(im*N*)Ru(SO$_4$)(NH$_3$)$_4$]Cl$_2$	340 [c] 410 [d]	0.04	[103]
trans-[Ru(HSO$_3$)(NH$_3$)$_4$(im*N*)]Cl		0.30	
trans-[Ru(SO$_4$)(NH$_3$)$_4$(im*N*)]Cl		−0.04	[103]
[≡Si(CH$_2$)$_3$(im*N*)Ru(NH$_3$)$_4$(py)]Cl	340 [a] 414 [b]	0.27	[103]
trans-[Ru(NH$_3$)$_4$(im*N*)(py)](PF$_6$)$_2$	482 [b]	0.25	[118–120]
[≡Si(CH$_2$)$_3$(im*N*)Ru(NO)(NH$_3$)$_4$]Cl$_2$	270 334		[103]
[≡Si(CH$_2$)$_3$(im*N*)Ru(NO$_2$)(NH$_3$)$_4$]Cl$_2$	330		
[≡Si(CH$_2$)$_3$(dpp)Ru(CO)(NH$_3$)$_4$]Cl$_2$	290 [b]		[3,121]
[≡Si(CH$_2$)$_3$(dpp)Ru(NH$_3$)$_4$(isn)]Cl$_2$	416 [b] 430 [b][4]		[3,121]
[≡Si(CH$_2$)$_3$(isn)Ru(NH$_3$)$_4$(SO$_2$)]Cl$_2$	270 378 [b]	0.62	[20]
trans-[Ru(isn)(NH$_3$)$_4$(SO$_2$)]Cl$_2$	268 356 [b]	0.64	[20]
[≡Si(CH$_2$)$_3$(isn)Ru(SO$_4$)(NH$_3$)$_4$]Cl$_2$	264 340 [c]	0.24	[20]
trans-[Ru(SO$_4$)(NH$_3$)$_4$(isn)]Cl	268 334 [c]	0.28	[73]
[≡Si(CH$_2$)$_3$(isn)Ru(H$_2$O)(NH$_3$)$_4$]Cl$_2$	274 492 [b]		[20]
trans-[Ru(H$_2$O)(NH$_3$)$_4$(isn)](PF$_6$)$_2$	266 486 [b]		[20,118]
[Ru(NH$_3$)$_5$(isn)](PF$_6$)$_2$	260 479 [b]		[122]
[≡Si(CH$_2$)$_3$(isn)Ru(NO)(NH$_3$)$_4$](PF$_6$)$_3$	274 334 [d,e]	−0.05	[20]

Table 3 (*Continued*)

Compound	λ_{max} [2] (nm)	E'_f V vs. NHE[3]	Ref.
trans-[Ru(NO)(NH_3)$_4$(isn)](BF_4)$_3$	268 323 [d,e] 486 [e]	0.00 [6]	[63]
SiO_2/*trans*-[Ru(NO)(Cl)(cyclam)](PF_6)$_2$	260 [b] 355 [d,e] 452 [e]	−0.12 [6]	[21]
SiO_2/SiSH/*trans*-[Ru(NO)(Cl)(cyclam)](PF_6)$_2$	270 310 367		[112]
SiO_2/$SiNH_2$/*trans*-[Ru(NO)(Cl)(cyclam)](PF_6)$_2$	269 350 [d,e] 481 [e]		[21]
SiO_2/SiPr/*trans*-[Ru(NO)(Cl)(cyclam)](PF_6)$_2$	270 [b] 320 [d,e]		[112]
trans-[Ru(NO)(Cl)(cyclam)](PF_6)$_2$	262 [b] 352 [d,e] 435 [e]	−0.10 [6]	[57]
SiO_2/[Ru(NO)(H_2O)(salen)]NO_3	390 [e]		[32]
[Ru(NO)(H_2O)(salen)](NO_3)	387 [e]		[32]
[≡TiORu(NH_3)$_5$]		0.02	[31]
[Ru(NH_3)$_5$(H_2O)](PF_6)$_3$		0.06	[31]
[≡TiClRu(NH_3)$_5$]		−0.04	[31]
[Ru(NH_3)$_5$Cl]$^{2+}$		−0.04	[31]
[≡TiOOs(NH_3)$_5$]		−0.91	[31]
[Os(NH_3)$_5$(H_2O)](PF_6)$_3$		−0.74	[31]
K_4[≡SiTiORu(CN)$_6$]	362 [b] 390 [b](sh)	0.97	[31,123]
K[≡SiTiO(CN)$_5$Ru(CN)Ru(NH_3)$_5$]	369 [b] 642 [f]	−0.01 [7] −0.49 [7]	[31,123]
Zn[≡SiTiO(CN)$_5$Ru(CN)Ru(NH_3)$_5$]	366 [b] 578 [f]	−0.02 [7] −0.81 [7]	[31,123]
K_4[Ru(CN)$_6$]	295 [d] 206 [b]	0.96	[124,125]
[(CN)$_5$Ru(CN)Ru(NH_3)$_5$]Cl	300 [b] 680 [f]	−0.01 −0.48	[31,123]
Zn[(CN)$_5$Ru(CN)Ru(NH_3)$_5$]$_2$	620 [f]	−0.017 −0.79	[31,123]
K_4[(4-PVP)[Ru(CN)$_6$]		0.92 [8]	[3,19]
[(4-PVP)Ru(NH_3)$_4$(SO_2)]Cl_2	400 [b](4)	0.43	[3,19]
[(4-PVP)Ru(NH_3)$_4$(pz)]Cl_2	476 [b](4)		[3,19]
[(4-PVP)Ru(CN)(NH_3)$_4$]Cl_2	435 [b](4)		[3,19]
[(4-PVP)Ru(NH_3)$_5$]Cl_2	383 [a]		[3,19]
[(4-PVP)Ru(H_2O)(NH_3)$_4$](PF_6)$_2$	406 [a]		[3,19]
trans-[Ru(NH_3)$_4$(py)(pz)](PF_6)$_2$	352 [a] 474 [b]		[120]
[Ru(NH_3)$_6$]–Y	270 [c]		[78,79]
[Ru(NH_3)$_6$]Cl_4	275 [c] 323 [d]		[124,125]
cis-[Ru(H_2O)$_2$(NH_3)$_4$](PF_6)$_2$	253 [c] 330 [d]		[76–79]
cis-[Ru(H_2O)$_2$(NH_3)$_4$]–Y	345 [d]		[76–79]
trans-[Ru(H_2O)(NH_3)$_4$(SO_2)]–Y	276 [c] 282 [c](g) 322 [d] 350 [d](5) 324 [d] 330 [d](h)	0.34 [7]	[76–79]

Table 3 (*Continued*)

Compound	λ_{max}[2] (nm)	E'_f V vs. NHE[3]	Ref.
trans-[Ru(H_2O)(NH_3)$_4$(SO_2)](tfms)$_2$	220 [c] 281 [d]	0.29 [7]	[76–79]
trans-[Ru(SO_3)(H_2O)(NH_3)$_4$](tfms)$_2$	250 [c] 343 [d]		[76–79]
trans-[Ru(H_2O)(NH_3)$_4$(P(OEt)$_3$)]–Y	327 [c] 329 [c](5) 360 [d] 364 [d](5)	0.65 [7]	[76–79]
trans-[Ru(H_2O)(NH_3)$_4$(P(OEt)$_3$)](PF_6)$_2$	316 [d]		[76–79]
[Ru(NH_3)$_5$(pz)]–Y	470 [b] 467 [b](5)		[76–79]
[Ru(NH_3)$_5$(pz)]Cl_2	474 [b]		[76–79]
[Ru(NH_3)$_5$(dtdp)](PF_6)$_2$	458 [b]		[76–79]
[Ru(NH_3)$_5$(dtdp)]–Y	472 [b]		[76–79]
[≡Si(AEATS)(edta)Ru(NO)]		−0.09	[7]
K[Ru(NO)(edta)]		−0.07	[117]
G_0/G_2/G_3[Ru(H_2O)(edta)]	282 [c] 352 [d]	0.04	[6]
G_0/G_2/G_3[Ru(NO)(edta)]		−0.08	[6]
[Ru(H_2O)(Hedta)]	280 [c] 350 [d]	0.04	[117]

[1]CCl_4 or $CHCl_3$ suspension, except where noted; [2]$\lambda_{max} \pm 5$ nm; [3]reported values were converted to NHE for comparison purposes; [4]diffuse reflectance; [5]photoacoustic spectroscopy; [6]E, {RuNO}$^{6/7}$; [7]anodic peak potential; [8]preconcentrated electrode; [a]Ru$\pi \rightarrow L_{support}$ MLCT, [b]Ru$\pi \rightarrow L_{ligand}$ MLCT; [c]L → Ru LMCT; [d]d → d; [e]Ruπ → NO MLCT; [f]Ru(II) → Ru(III) MMCT; [g]pH 2.0; [h]pH 5.5; [sh]shoulder;.

trivalent aluminum cannot be ruled out. Therefore this interaction would increase the π acidity of the pyrazine ligand and induce a red shift of MLCT Ru(II) → pz MLCT band.

The electronic spectra of PLGA microparticles in aqueous solution exhibit a broad absorption band in the UV region. Thus, because both polymer and complex UV–vis absorption bands are located in the same region of the spectrum, in addition to light scattering, it is not possible to distinguish the complex bands when it is incorporated into the MP [14].

3.4. Electrochemistry

The modified carbon paste electrodes used to study solid materials are prepared by mixing carbon powder with the solid containing the electroative species and drops of mineral oil (Nujol) as aglutinant [4].

Generally, the metal-centered redox potentials for the Ru^{III}/Ru^{II} couple and for the {RuNO}$^{6/7}$ processes in immobilized complexes are experimentally identical to those observed for the analogous species in solution under similar experimental conditions (Table 3). This can be observed in the electrochemical behavior of the immobilized [≡Si(CH_2)$_3$(L)Ru(NH_3)$_4$(L′)]$^{2+}$ (L = isn, im*N*; L′ = H_2O, py, pz, SO_2, or pz) system, as exemplified by cyclic voltammogram of the L = im*N*, L′ = py system where only one reversible couple attributed to Ru^{III}/Ru^{II} is observed. This is similar to that which occurs for the non-immobilized complexes in solution [4,103]. A slight shift always smaller than 30 mV is observed in the potential values of the immobilized species relative to those of the ions in solution.

The sulfato derivative [4,103], easily obtained by oxidation of the immobilized ruthenium complex in the systems [≡Si(CH_2)$_3$(L)Ru(NH_3)$_4$(SO_2)] (L = im*N* and isn) by H_2O_2, exhibited the same characteristics observed in solution [103], showing an irreversible behavior due to the fast aquation of sulfate after reduction of the Ru(III) center [71,73]. The specific rate constant value at 25 °C, $k_{SO4}{}^{2-}$, for *trans*-[Ru(NH_3)$_4$(L)(SO_4)] is 16 s^{-1} for L = im*N* and isn [71]. Thus, in the time scale of the experiments, the starting species [≡Si(CH_2)$_3$(L)Ru(NH_3)$_4$(SO_4)]Cl was converted to [≡Si(CH_2)$_3$(L)Ru(H_2O)(NH_3)$_4$] (L = im*N* and isn) [4,20,103] in the electrode.

The modified electrodes using these ruthenium tetraammines immobilized on silica gel or 4-PVP allows evaluation of the pK_{a1} and pK_{a2} values of 2.1 and 6.0, respectively, for the acid–base equilibrium of the ligand SO_2 Eqs. (10) and (11) [103] following the pH-dependent redox potentials.

$$[\equiv Si(CH_2)_3(imN)Ru(NH_3)_4(SO_2)]^{2+} + H_2O \overset{pK_{a1}}{\rightleftharpoons} [\equiv Si(CH_2)_3(imN)Ru(NH_3)_4(HSO_3)]^{+} + H_3O^{+} \quad (10)$$

$$[\equiv Si(CH_2)_3(imN)Ru(NH_3)_4(HSO_3)]^{+} + H_2O \overset{pK_{a2}}{\rightleftharpoons} [\equiv Si(CH_2)_3(imN)Ru(NH_3)_4(SO_3)] + H_3O^{+} \quad (11)$$

These pK_a values are comparable with those observed by Isied and Taube for the *trans*-[Ru(H_2O)(NH_3)$_4$(SO_2)]$^{2+}$ complex in solution (pK_1 2.15 and pK_2 5.05) [72] for Eqs. (10) and (11). Since the Ru(III) species are more acidic than the corresponding Ru(II) complex, the pK_a for the oxidized species are below the investigated pH range. The same behavior is observed for *trans*-[Ru(H_2O)(NH_3)$_4$(SO_2)]Cl_2 immobilized in the 4-PVP polymer [3]. In this system, the calculated pK_a values for equations 11 and 12 are 2.4 ± 0.2 and 4.4 ± 0.4 respectively, which are near the calculated values (1.7 ± 0.1 and 4.9 ± 0.1) for the *trans*-[Ru(NH_3)$_4$(SO_2)(py)]$^{2+}$complex in solution [72].

Differential pulse voltammograms of the 4-PVP modified electrode preconcentrated with the aquo complex *trans*-[Ru(H_2O)(NH_3)$_4$(SO_2)](tfms)$_2$ give E_p values shifted by 100 mV to more positive potentials relative to those observed for the same complex in solution [19]. This behavior is expected due to the presence of a pyridine ring in the polymer, which stabilizes the

Ru(II) center relative to the Ru(III) center through back-bonding interaction, indicating that the immobilization of this compound occurs by coordination to the 4-PVP nitrogen. Contrary to that described above, an electrostatic interaction is dominant in the $K_4[(4\text{-PVP})Ru(CN)_6]$ system [3]. In this latter case, similar $E_{1/2}$ values for the Ru^{III}/Ru^{II} couples are observed for the pre-concentrated modified electrode (0.92 V) and in solution studies (0.96 V).

There is only one Ru^{III}/Ru^{II} process for $[\equiv SiTiClRu(NH_3)_5]$ in solution [130,131] during the cathodic scan of $[Ru(NH_3)_5Cl]^{2+}$ ($E_{1/2} = -0.04$ V), but there are two redox processes at $E_{1/2} = -0.04$ and 0.06 V during the anodic scan. One is due to the oxidation of the remaining chloride species; the other is generated by the aquo species according to:

$$[Ru(NH_3)_5Cl]^{2+} + e^- \xrightarrow{E_{1/2}=-0.04V} [Ru(NH_3)_5Cl]^{+} + H_2O \longrightarrow [Ru(NH_3)_5(H_2O)]^{2+} + Cl^-$$

$$[Ru(NH_3)_5(H_2O)]^{2+} \xrightarrow{E_{1/2}=0.06V,\ -e^-} [Ru(NH_3)_5(H_2O)]^{3+}$$

However, for the complex immobilized on the silica surface there is only one Ru^{III}/Ru^{II} couple with $E_{1/2} = -0.04$ V [31]. Thus, unlike what was observed for the immobilized sulfate system [103], in which SO_4^{2-} is easily substituted, generating the aquo species upon reduction, the chloride ion remains coordinated after the metal center reduction on the matrix surface. This different behavior of $[\equiv SiTiClRu(NH_3)_5Cl]$ relative to SO_4^{2-} in $[\equiv Si(CH_2)_3(imN)Ru(SO_4)(NH_3)_4]Cl$ [31] is attributed to a direct interaction of the Cl^- ligand, which acts as a Ti-Cl-Ru bridge. In the case of the SO_4^{2-} system there is no bridge formation, since the interaction with the matrix is through the im*N* ligand [103].

Another interesting characteristic assigned to the matrix effect of an immobilized system compared with the behavior in solution is the observed inability of ClO_4^- ions to oxidize Ru^{II} [130]. In solution, [132] the reaction (Eq. (12))

$$8\,[Ru(NH_3)_5(H_2O)]^{2+} + ClO_4^- + 8\,H^+ \rightleftharpoons 8\,[Ru(NH_3)_5(H_2O)]^{3+} + Cl^- + 4\,H_2O \quad (12)$$

is described to be first order in [Ru(II)] and in $[ClO_4^-]$ and zero order in $[H^+]$ (in the range from 10^{-3} to 10^{-2} M) and occurs with $k = 2.6 \pm 0.1 \times 10^{-2}\ M^{-1}$. In the solid state, the reactants, ruthenium centers and perchlorate, are far away from each other and immobilized to afford the series of reactions necessary to convert ClO_4^- into Cl^- in the time scale of the experiment.

When in solution, nitrosyl ruthenium ammines, such as *trans*-$[Ru(NO)(NH_3)_4(L)]^{n+}$ (L = N heterocyclic bases) [58,63,111] complexes and others with chelating ligands as edta [117] and cyclam [57], show a reduction peak corresponding to the $\{RuNO\}^{6/7}$ process, which has been assumed to be mainly centered on the nitrosyl group (NO^+/NO^0 process). Also, for the immobilized $[\equiv Si(CH_2)_3(isn)Ru(NO)(NH_3)_4]^{3+}$ and [Ru(NO)(Hedta)] systems there is only one redox couple, attributed to the nitrosyl-centered reduction, $\{RuNO\}^{6/7}$ (Table 3).

The immobilization of K[Ru(Cl)(Hedta)] onto/into PAMAM (three generations G_x/Ru ($x = 0$, 2, and 3)) through a peptide-type bond generates the aquo species, [Ru(edta) (H_2O)] on the dendrimer ending groups, which upon reaction with NO form their nitrosyl analogues, G_x/RuNO. As observed for the silica gel system, only the process attributed to Ru^{III}/Ru^{II} and the $\{RuNO\}^{6/7}$ redox couples are observed in the voltammograms of the aquo and nitrosyl immobilized derivatives, respectively.

The immobilized nitrosyl ruthenium ammine $[\equiv Si(CH_2)_3(isn)Ru(NO)(NH_3)_4](PF_6)_3$ displays a cathodic peak similar to that of the complex in solution (Table 3). This reduction involves the release of NO and formation of the aquo species. Aquation of the coordinated nitrosyl in $[\equiv Si(CH_2)_3(isn)Ru(NO)(NH_3)_4](PF_6)_3$ after monoelectronic reduction was also investigated using Eu^{2+} ions as the chemical reducing agent, and the reaction was monitored by vibrational and electronic spectroscopy and with an NO selective electrode. After reduction of the immobilized complex, ν(NO) is completely suppressed and the UV–vis spectrum of the resulting material showed a band at 486 nm, which is in agreement with that observed for the *trans*-$[Ru(isn)(NH_3)_4(H_2O)]^{2+}$ complex and $[\equiv Si(CH_2)_3(isn)Ru(NH_3)_4(H_2O)]^{2+}$. In addition, NO concentrations calculated using the NO selective electrode were in good agreement with the expected value based on the ruthenium content [20].

After one-electron reduction ($E_{NO+/NO} = -0.07$ V vs. NHE), the $[Ru(NO)(edta)]^-$ complex releases NO ($k = 2.1 \pm 0.4 \times 10^{-3}\ s^{-1}$) [117]. Furthermore, the $[Ru(H_2O)(edta)]^{2-}$ species formed is able to quickly substitute the H_2O ligand for NO_2^-, yielding $[Ru(edta)(NO_2)]^{3-}$ ($t_{1/2} < 60$ s for 0.01 M $NaNO_2$ solution). The rate for conversion of the nitrite species into the nitrosyl one is not yet available, but by analogy with systems it is expected to be fast ($t_{1/2} \ll 1$ s). Since the predominant species when pH < 10 is $[Ru(NO)(edta)]^-$, the fast and quantitative conversion of $[Ru(edta)(NO_2)]^{3+}$ into the nitrosyl form is assumed to occur in a large pH range. Therefore, the $[Ru^{III}(H_2O)(edta)]^-/[Ru^{II}(NO)(edta)]^-$ system would behave as an NO buffer, according to the cycle shown in Scheme 5. Based on the accumulated knowledge of the solution chemistry of this system, the rate determining step of this cycle is expected to be the aquation of the coordinated NO ($k_{NO} = 2.1 \times 10^{-3}\ s^{-1}$). The catalytic Ru(II) center behavior has also been demonstrated for the *trans*-$[Ru(H_2O)(NH_3)_4(isn)]^{2+}$ and $[\equiv Si(CH_2)_3(isn)Ru(H_2O)(NH_3)_4]^{2+}$ systems, for which, as in the case of the edta complex, the predominant species below pH 10 is *trans*-$[Ru(NO)(NH_3)_4(isn)]^{3+}$. An interesting property that immobilization could offer over the solution system is the possibility to locate the immobilized material in a specific target site and even recover the material from the medium at any time. This may be extremely useful for biological applications in situations where constant local concentrations of NO are desired, as in the case of drug eluting stents to prevent resthenosis. This is because no significant leaching of the immobilized compound is

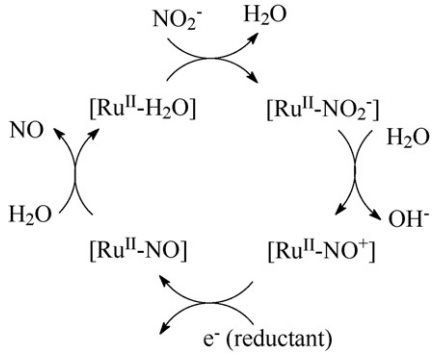

Scheme 5. Catalytic cycle for conversion of NO_2^- into NO^+ by immobilized Ru complexes on modified silica surface [7,20] or PAMAM dendrimer [6].

observed after catalytic cycles of NO_2^- conversion, and considering that NO_2^- is the largest pool of NO_x species in the blood, in the presence of a suitable biological reducing agent this material can thus generate NO from NO_2^-, according to the cycle in Scheme 5. In other words, this material can turn out to be a long-lasting NO generator.

As for $[\equiv Si(CH_2)_3(isn)Ru(NH_3)_4(NO)]^{3+}$, the immobilization of *trans*-$[Ru(NO)Cl(cyclam)](PF_6)_2$ in the SiO_2 matrix (xerogel) does not significantly affect the $\{RuNO\}^{6/7}$ reduction potentials (Table 3).

Complexes of the $[Ru(NH_3)_4L_1L_2]^{n+}$ type, (where $L_1 = NH_3$ or SO_4^{2-}, and $L_2 = NH_3$, H_2O, pz or dtdp) immobilized into the zeolite cavity [76–79] show $E_{1/2}$ shifts around 65 mV to more negative potentials (Table 3) relative to the system in solution. This shift is attributed to the stabilization of the Ru(III) oxidation state over Ru(II). Also, the evaluation of the currents in the pulse differential voltammograms shows that the complexes, except for $[Ru(NH_3)_6]$–Y, are lixiviated from the cavity within around 1 h.

Nitro ruthenium complexes, such as *cis*-$[Ru(NO_2)(bpy)_2(4\text{-pic})](PF_6)_2$, have also been investigated as NO donors. This complex has a pH-dependent behavior; the predominant species are the nitro form at pH ≥ 5.0 and the nitrosyl at pH ≤ 5.0. The nitrosyl form reduction potential is 0.3 V vs. NHE. Upon reduction, the nitrosyl species releases NO. The results of the topical administration of the gels containing this complex are consistent with NO release. The aquo form, which results from its reduction, has been observed by HPLC. Since the parent complex is inert with regard to ligand substitution, the aquo form should come from the release of NO, and, thus, from the reduction of *cis*-$[Ru(NO)(bpy)_2(4\text{-pic})]^{3+}$ by a reducing agent present in the skin.

3.5. Scanning electron microscopy and other spectroscopic methods

The characterization of *trans*-$[Ru(NO)(NH_3)_4(py)](BF_4)_3$ immobilized in PLGA microparticles was achieved by means of scanning electron microscopy (SEM) (Fig. 2) and energy dispersive spectroscopy (EDS), since vibrational spectroscopy does not give much information about this system. According to SEM images, the prepared particles are spherical in shape, with smooth surface. There are no significant differences between empty PLGA particles and those containing *trans*-$[Ru(NO)(NH_3)_4(py)](BF_4)_3$. The EDS spectrum of the loaded microparticle gives a typical ruthenium energy value of 2.55 keV [14], indicating that the complex is present in the microparticle.

The xerogel material obtained by entrapment of *trans*-$[Ru(NO)Cl(cyclam)](PF_6)_2$, was also characterized by means of ^{13}C and ^{29}Si high resolution solid-state NMR with the magic angle spinning technique (MAS), SEM using EDS detector to map Si and Cl in the material, and X-ray photoelectron microscopy (XPS). The ^{29}Si NMR spectra indicate that the condensation of the hydrolyzed tetraethylorthosilicate is not hindered by the presence of the complex, resulting in a highly interconnected three-dimensional SiO_2 network. From the ^{13}C CP-MAS NMR spectra of *trans*-$[Ru(NO)Cl(cyclam)](PF_6)_2$ entrapped into SiO_2, it is possible to identify, the peaks of $-CH_2$ of the cyclam ring in the region of 10–70 ppm [21]. EDS mapping reveals a homogenous distribution of the ruthenium complex in the material. The similarities between the IR spectra of the entrapped and non-entrapped *trans*-$[Ru(NO)Cl(cyclam)](PF_6)_2$ are in agreement with similar XPS binding energies observed for Ru $3d_{5/2}$ (282.1 eV) and N 1 s (397.6 eV) XP-peaks of SiO_2/*trans*-$[Ru(NO)Cl(cyclam)](PF_6)_2$ and those of the bulk *trans*-$[Ru(NO)Cl(cyclam)](PF_6)_2$ with Ru $3d_{5/2}$ (282.1 eV) and N 1s (399.4 eV) [21].

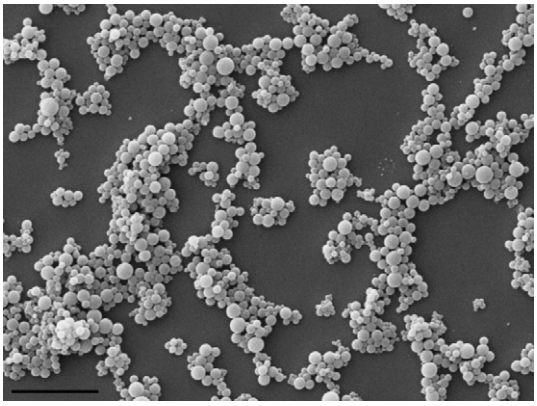

Fig. 2. Scanning electron micrographs of nanoparticles loaded with *trans*-$[Ru(NO)(NH_3)_4(py)](BF_4)_3$, prepared by the double evaporation method. The original magnification was 2500×. The scale bar is equal to 10 μm.

3.6. Photochemistry of immobilized compounds

The NO release by irradiation with light can potentially be used as a biological tool and in clinical therapies such as in photodynamic therapy (PDT), which has been a major theme in several different research groups [133–146] and also is one of our research goals [14,32,58–60,128,147–152]. Ruthenium nitrosyls can release NO by reduction or photochemical reactions, which are not exclusive. That means, that depending on the $\{RuNO\}^{6/7}$ reduction potential and UV–vis spectra, they can release NO by both ways or by either one. One complex can release NO at a certain irradiation wavelength and not be reduced; conversely it can be reduced but be photochemically inactive at a particular wavelength or in the absence of irradiation. For biological applications, following intrabody administration, complex activation for NO release should preferentially occur by reduction, and the complex can be activated or not depending on the potential. On the other hand, for topical and intradermal applications as in dermatology, for instance, or PDT, activation can be achieved by irradiation without the need for a chemical reducing agent. In the latter case, efforts have been devoted toward the development of systems capable of releasing NO in the therapeutic window (800–1200 nm). The reduction potentials and the spectra for Ru nitrosyls can be tuned by the judicious choice of ligands, as already shown [58,129]. Photochemically, Ru am(m)ine nitrosyls release NO in solution by undergoing only one reaction, as shown in Eq. (13) [14,149].

$$\textit{trans}\text{-}[Ru(NO)(NH_3)_4(py)]^{3+} \xrightarrow{h\nu} \textit{trans}\text{-}[Ru(H_2O)(NH_3)_4(py)]^{3+} + NO \quad (13)$$

Immobilization of the complexes does not alter the photochemical behavior of those complexes regarding NO release. The *trans*-$[Ru(NO)Cl(cyclam)](PF_6)_2$ and $[Ru(salen)(OH_2)(NO)]NO_3$ complexes entrapped into xerogel matrices have optical transparency, which allows for their irradiation with light. When the vitreous $[Ru(salen)(OH_2)(NO)]NO_3$ derived material is photolyzed with an IR-filtered 150 W Xenon lamp the intensity of the 1856 cm^{-1} ν(NO) band in the IR spectra decreases consistent with the photochemical labilization of the coordinated NO, as confirmed by trapping with $[Ru(Hedta)(OH_2)]$ solution and formation of the Ru(III) salen photoproduct [32]. A similar behavior is observed upon irradiation of the SiO_2/*trans*-$[Ru(NO)Cl(cyclam)](PF_6)_2$ xerogel with 334 nm light [21]. In both cases, the nitrosyl complex can be regenerated after NO photorelease. While the regeneration of entrapped ruthenium salen complex is achieved by immersing the material into a neutral nitrite aqueous solution (with or without prior reduction with Eu^{2+} ions), Eqs. (14) and (15), the ruthenium

cyclam complex in SiO_2 matrix is reacted with $NO_{(g)}$ resulting in SiO_2/*trans*-[Ru(NO)Cl(cyclam)]$(PF_6)_2$ Eqs. (16) and (17).

$$SiO_2/[Ru(NO)(H_2O)(salen)](NO_3) \xrightarrow{h\nu} SiO_2/[Ru(X)(H_2O)(salen)](NO_3) + NO_{(g)} \quad (14)$$

$$SiO_2/[Ru(X)(H_2O)(salen)](NO_3) \xrightarrow{NO^-_{2(aq)}} SiO_2/[Ru(NO)(H_2O)(salen)](NO_3) \quad (15)$$

$$SiO_2/trans-[Ru(NO)Cl(cyclam)](PF_6)_2 \xrightarrow{h\nu} SiO_2/trans\text{-}[Ru(OH)Cl(cyclam)](PF_6)_2 + NO_{(g)} \quad (16)$$

$$SiO_2/trans-[Ru(NO)Cl(cyclam)](PF_6)_2 \xrightarrow{NO_{(g)}} SiO_2/trans\text{-}[Ru(OH)Cl(cyclam)](PF_6)_2 \quad (17)$$

Nitric oxide release from the xerogel-based material and a metal complex is also observed in a photoactive manganese nitrosyl $[Mn(PaPy_3)(NO)]ClO_4$ ($PaPy_3H$ = *N*,*N*-bis-(2-pyridylmethyl)amine-*N*-ethyl-2-pyridine-2-carboxamide) upon visible light irradiation [138].

The nitric oxide release from $[\equiv Si(CH_2)_3(isn)Ru(NH_3)_4(NO)]^{3+}$ was also investigated by means of irradiation with light. As observed for ruthenium nitrosyl complexes entrapped into xerogel matrices, irradiation of the immobilized $[\equiv Si(CH_2)_3(isn)Ru(NH_3)_4(NO)]^{3+}$ complex with IR filtered 150 W Xenon Lamp (or monochromatic light of 334 nm) results in NO photochemical labilization. After direct photolysis of the $[\equiv Si(CH_2)_3(isn)Ru(NH_3)_4(NO)]^{3+}$ dispersed in KBr pellet, the resulting NO-depleted material was reacted with neutral nitrite aqueous solution, resulting in the ready regeneration of immobilized ruthenium nitrosyl tetraammine [20]. This reaction occurs in the time scale of seconds, whereas for the xerogel matrices it occurs in the time scale of several hours, as judged by UV–vis and IR spectra [32].

Other systems based on light stimulation have also been proposed for NO production from metal nitrosyls. Ford et al. have developed a strategy for the photosensitized release of NO using CdSe/ZnS water-soluble quantum dots (QD) as antennae for energy transfer to *trans*-$[Cr(cyclam)(ONO)_2]^+$, a known photochemical NO precursor [153,154]. Under irradiation, NO production is ~15-fold enhanced with a QD/complex ratio of 10^{-3} regarding the amount of NO produced from the *trans*-$[Cr(cyclam)(ONO)_2]^+$ solution only.

The reactivity of PLGA encapsulated and free *trans*-$[Ru(NO)(NH_3)_4(py)](BF_4)_3$ complex was investigated by means of biological assays with and without light irradiation.

In the absence of light irradiation, the nitrosyl complex *trans*-$[Ru(NO)(NH_3)_4(py)](BF_4)_3$ in solution has low toxicity toward B16-F10 murine cells at concentrations lower than 1×10^{-4} M, but it is toxic at $>1 \times 10^{-3}$ M, with cell death being attributed to NO release following reduction of the complex in the cell environment. The encapsulated *trans*-$[Ru(NO)(NH_3)_4(py)](BF_4)_3$ (pyMP) does not show toxicity, which is attributed to the lower bioavailability and availability of the entrapped complex to the medium and its reducing agents. However, upon light irradiation, pyMP is able to release sufficient NO, which in turn can diffuse out of the matrix, reach the adjacent cell membranes, and kill the tumor cell [14]. This illustrates that systems of this type can deliver NO locally, at high (or desirable) concentrations [14].

NO photoproduction by light irradiation of $[Ru(terpy)(L))NO]^{3+}$ (L = NH.NHq and bipy) entrapped into a sol–gel matrix and in aqueous solution has also been described [28]. Similar results have also been obtained from *trans*-$[RuCl([15]aneN_4)(NO)]^{2+}$ by photoinduced electron transfer with visible light in the presence of a sensitizer. In these cases, $[Ru(NH_3)_5(pz)]^{2+}$ was used as light irradiation antenna in a phosphate buffer solution pH 7.4, and also in water/oil emulsion, sol–gel, and silicone membrane [86]. The quantitative behavior of this system suggests that the two cations undergo interaction so that photoexcitation of the visible absorbing $[Ru(NH_3)_5(pz)]^{2+}$ is followed by electron or energy transfer to *trans*-$[RuCl([15]aneN_4)NO]^{2+}$, which does not absorb appreciably at the excitation wavelength, thereby leading to NO release from the reduced nitrosyl complex. Although all the three studied delivery systems involving *trans*-$[RuCl([15]aneN_4)NO]^{2+}$ and $[Ru(NH_3)_5(pz)]^{2+}$ have resulted in NO release, the stability of the mixture of the ruthenium complexes in water/oil emulsion is limited. The complexes show appreciable release from emulsion after 2 h, although this is not observed when sol–gel and silicone matrices are used to entrap the complexes, as also verified for $[Ru(terpy)(NH.NHq)NO]^{3+}$. The continuous NO release from solid membrane implies consumption of *trans*-$[Ru(NO)Cl([15]aneN_4)]^{2+}$ and oxidation of $[Ru(NH_3)_5(pz)]^{2+}$, while the membrane color changes from deep red to white.

4. Concluding remarks

Procedures for the immobilization of ruthenium complexes have been successfully tested and the reactivity of these compound has been verified. Generally speaking, according to the accumulated data from IR, UV–vis, and EPR spectra, and electrochemical measurements, the immobilization of precursors into/onto modified silica gel, 4-PVP, zeolites, dendrimers, hydrogel, membranes, and PLGA nano and microparticles does not alter significantly the properties of the complexes. One exception is when the reaction involves more than two particules as in the cases of ClO_4^- reduction and chloride aquation, where Cl^- acts as a bridge between the ruthenium metal center and the support. When the complex is immobilized into the zeolite cage, some degree of stabilization of the oxidation state (III) compared with (II) is observed for the ruthenium complexes.

Therefore, at least as far as our compounds are concerned, the chemical behavior of these complexes in solution and immobilized into/onto matrices is quite similar. This is a very interesting and useful approach for tailoring homogeneous catalysts via their immobilization.

This would be the case of catalytic cycles for nitrite/nitrosonium conversion, which holds a promissing potential for biological applications. Controlling matrix properties and shape may allow for additional control of the properties of the immobilized complex.

Acknowledgements

The authors thank grants and fellowships from the Brazilian agencies FAPESP, CAPES, and CNPq. They also thank Ms Cynthia Maria de Campos Prado Manso for the English revision.

References

[1] Y. Gushikem, C.R.M. Peixoto, U.P. Rodrigues, L.T. Kubota, E. Stadler, J. Colloid Interface Sci. 184 (1996) 236.
[2] S. Denofre, Y. Gushikem, S.C. Decastro, Y. Kawano, J. Chem. Soc. Faraday Trans. 89 (1993) 1057.
[3] M.T. Hoffmann, S.M.C. Neiva, M.R. Martins, D.W. Franco, Anchoring and reactivity of ruthenium tetraammines on silica and 4(vinylpyridine), in: H.A. Mottola, J.R. Steinmetz (Eds.), Chemically Modified Surfaces, Elsevier, Amsterdam, 1992.
[4] S.M.C. Neiva, J.A.V. Santos, J.C. Moreira, Y. Gushikem, H. Vargas, D.W. Franco, Langmuir 9 (1993) 2982.
[5] L.T. Kubota, Y. Gushikem, Electrochim. Acta 37 (1992) 2477.
[6] P.G.Z. Benini, B.R. McGarvey, D.W. Franco, Nitric Oxide 19 (2008) 245.

[7] P.G. Zanichelli, R.L. Sernaglia, D.W. Franco, Langmuir 22 (2006) 203.
[8] P. Mastrorilli, C.F. Nobile, Coord. Chem. Rev. 248 (2004) 377.
[9] S. Syukri, A. Sakthivel, W. Sun, F. Kuhn, Catal. Lett. 128 (2009) 18.
[10] F.C. Gong, D.X. Wu, Z. Cao, X.C. He, Biosens. Bioelectron. 22 (2006) 423.
[11] R.D.S. Luz, F.S. Damos, A.A. Tanaka, L.T. Kubota, Sens. Actuators B-Chem. 114 (2006) 1019.
[12] N.K. Chaudhury, R. Gupta, S. Gulia, Defence Sci. J. 57 (2007) 241.
[13] K.C. Gupta, A.K. Sutar, J. Macromol. Sci. Part A Pure Appl. Chem. 44 (2007) 1171.
[14] A.J. Gomes, P.A. Barbougli, E.M. Espreafico, E. Tfouni, J. Inorg. Biochem. 102 (2008) 757.
[15] G.M. Halpenny, M.M. Olmstead, P.K. Mascharak, Inorg. Chem. 46 (2007) 6601.
[16] S. Hwang, M.E. Meyerhoff, Biomaterials 29 (2008) 2443.
[17] B.K. Oh, M.E. Meyerhoff, Biomaterials 25 (2004) 283.
[18] K.P. Dobmeier, D.A. Riccio, M.H. Schoenfisch, Anal. Chem. 80 (2008) 1247.
[19] M.T. Hoffmann, B.S. Lima Neto, A.M.G. Massabni, D.W. Franco, J. Inorg. Org. Pol. 3 (1993) 41.
[20] F.G. Doro, U.P. Rodrigues, E. Tfouni, J. Colloid Interface Sci. 307 (2007) 405.
[21] K.Q. Ferreira, J.F. Schneider, P.A.P. Nascente, U.P. Rodrigues, E. Tfouni, J. Colloid Interface Sci. 300 (2006) 543.
[22] J.A.A. Sales, F.P. Faria, A.G.S. Prado, C. Airoldi, Polyhedron 23 (2004) 719.
[23] A. Schiller, R. Scopelliti, K. Severin, Dalton Trans. (2006) 3858.
[24] M.R. Buchmeiser (Ed.), Polymeric Materials in Organic Synthesis and Catalysis, Wiley-VCH, 2003.
[25] M. Rosso-Vasic, L. De Cola, H. Zuilhof, J. Phys. Chem. C 113 (2009) 2235.
[26] L. Gorton (Ed.), Biosensors and Modern Biospecific Analytical Techniques, Elsevier, 2005.
[27] M. Vaccaro, R. Del Litto, G. Mangiapia, A.M. Carnerup, G. D'Errico, F. Ruffo, L. Paduano, Chem. Commun. (2009) 1404.
[28] R.G. de Lima, M.G. Sauaia, C.Z. Ferezin, L.M. Pepe, N.M. Jose, L.M. Bendhack, Z.N. da Rocha, R.S. Silva, Polyhedron 26 (2007) 4620.
[29] R.K. Iller, The Chemistry of Silica, Wiley, New York, 1979.
[30] H.A. Montola, J.R. Steimetz (Eds.), Chemically Modified Surfaces, Elsevier, New York, 1992.
[31] D.R. do Carmo, U.P. Rodrigues, Y. Gushikem, D.W. Franco, Polyhedron 19 (2000) 2277.
[32] J. Bordini, P.C. Ford, E. Tfouni, Chem. Commun. (2005) 4169.
[33] C.J. Brinker, G.W. Scherrer, Sol-Gel Science the Physics and Chemistry of Sol Gel Processing, Academic, San Diego, 1990.
[34] H. Schmidt, J. Non-Cryst. Solids 100 (1988) 51.
[35] D. Avnir, T. Coradin, O. Lev, J. Livage, J. Mater. Chem. 16 (2006) 1013.
[36] C.R. McMillin, Rubber Chem. Technol. 79 (2006) 500.
[37] K.A. Mowery, M.H. Schoenfisch, J.E. Saavedra, L.K. Keefer, M.E. Meyerhoff, Biomaterials 21 (2000) 9.
[38] C.M. Hassan, N.A. Peppas, Biopolymers/Pva Hydrogels/Anionic Polymerisation Nanocomposites, Springer-Verlag, 2000.
[39] A.J. Gomes, C.N. Lunardi, A.C. Tedesco, Photomed. Laser Surg. 25 (2007) 428.
[40] A.J. Gomes, R.M.N. Assuncao, G. Rodrigues, E.M. Espreafico, A.E.D. Machado, J. Appl. Polym. Sci. 105 (2007) 964.
[41] A.J. Gomes, A.S. Faustino, A.E.H. Machado, M.E.D. Zaniquelli, T.D. Rigoletto, C.N. Lunardi, L.O. Lunardi, Drug Deliv. 13 (2006) 447.
[42] D.A. Ossipov, S. Piskounova, J. Hilborn, Macromolecules 41 (2008) 3971.
[43] A.V. Deshpande, U. Kumar, J. Non-Cryst. Solids 306 (2002) 149.
[44] N.A. Stasko, M.H. Schoenfisch, J. Am. Chem. Soc. 128 (2006) 8265.
[45] E. Chiellini, R. Solaro, Adv. Mater. 8 (1996) 305.
[46] L.L. Hench, J.K. West, Chem. Rev. 90 (1990) 33.
[47] S.M. Nie, Y. Ching, G.J. Kim, J.W. Simons, Annu. Rev. Biomed. Eng. 9 (2007) 257.
[48] P. Pacher, J.S. Beckman, L. Liaudet, Physiol. Rev. 87 (2007) 315.
[49] L.J. Ignarro, Nitric Oxide: Biology and Pathobiology, Academic Press, USA, 2000.
[50] D.A. Wink, M.B. Grisham, J.B. Mitchel, P.C. Ford, Nitric Oxide Pt. A 268 (1996) 12.
[51] D.A. Wink, J.F. Darbyshire, R.W. Nims, J.E. Saavedra, P.C. Ford, Chem. Res. Toxicol. 6 (1993) 23.
[52] M.M. Reynolds, J.A. Hrabie, B.K. Oh, J.K. Politis, M.L. Citro, L.K. Keefer, M.E. Meyerhoff, Biomacromolecules 7 (2006) 987.
[53] S.M. Marxer, A.R. Rothrock, B.J. Nablo, M.E. Robbins, M.H. Schoenfisch, Chem. Mater. 15 (2003) 4193.
[54] M.E. Robbins, M.H. Schoenfisch, J. Am. Chem. Soc. 125 (2003) 6068.
[55] J.T. Mitchell-Koch, T.M. Reed, A.S. Borovik, Angew. Chem. Int. Ed. 43 (2004) 2806.
[56] C.R. Pestana, D.P.S. Phelippin, A.C.M. Polizello, D.J. Dorta, S.A. Uyemura, A.C. Santos, F.G. Doro, F.P. Rodrigues, E. Tfouni, C. Curti, Nitric Oxide 20 (2009) 24.
[57] D.R. Lang, J.A. Davis, L.G.F. Lopes, A.A. Ferro, L.C.G. Vasconcellos, D.W. Franco, E. Tfouni, A. Wieraszko, M.J. Clarke, Inorg. Chem. 39 (2000) 2294.
[58] E. Tfouni, M. Krieger, B.R. McGarvey, D.W. Franco, Coord. Chem. Rev. 236 (2003) 57.
[59] F.S. Oliveira, V. Togniolo, T. Pupo, A.C. Tedesco, R.S. da Silva, Inorg. Chem. Commun. 7 (2004) 160.
[60] Z.N. da Rocha, M.S.P. Marchesi, J.C. Molin, C.N. Lunardi, K.M. Miranda, L.M. Bendhack, P.C. Ford, R.S. da Silva, Dalton Trans. (2008) 4282.
[61] J.J.J. Silva, A.L. Osakabe, W.R. Pavanelli, J.S. Silva, D.W. Franco, Br. J. Pharmacol. 152 (2007) 112.
[62] P.G. Zanichelli, H.F.G. Estrela, R.C. Spadari-Bratfisch, D.M. Grassi-Kassisse, D.W. Franco, Nitric Oxide 16 (2007) 189.
[63] S.D.S. Borges, C.U. Davanzo, E.E. Castellano, J. Schpector, S.C. Silva, D.W. Franco, Inorg. Chem. 37 (1998) 2670.
[64] A.S. Torsoni, B.F. de Barros, J.C. Toledo, M. Haun, M.H. Krieger, E. Tfouni, D.W. Franco, Nitric Oxide 6 (2002) 247.
[65] H.J. Xu, Y. Cheng, J.F. Sun, B.A. Dougan, Y.Z. Li, X.T. Chen, Z.L. Xue, J. Organomet. Chem. 693 (2008) 3851.
[66] A.S. Amarasekara, A.R. Oki, I. McNeal, U. Uzoezie, Catal. Commun. 8 (2007) 1132.
[67] W.S. Cardoso, M.S.P. Francisco, R. Landers, Y. Gushikem, Electrochim. Acta 50 (2005) 4378.
[68] P.K. Jal, S. Patel, B. Mishra, Talanta 62 (2004) 1005.
[69] K. Kupiec, P. Konieczka, J. Namiesnik, Crit. Rev. Anal. Chem. 39 (2009) 60.
[70] L.C. Codognoto, P.G. Zanichelli, R.L. Sernaglia, J. Braz. Chem. Soc. 16 (2005) 620.
[71] H.A.D. Silva, B.R. McGarvey, R.H.D. Santos, M. Bertotti, V. Mori, D.W. Franco, Can. J. Chem. 79 (2001) 679.
[72] S. Isied, H. Taube, Inorg. Chem. 13 (1974) 1545.
[73] H.A.S. Silva, R.M. Carlos, A.J. Camargo, C.M.C. Picchi, R.H.D. Santos, B.R. McGarvey, D.W. Franco, Inorg. Chim. Acta 357 (2004) 3147.
[74] P.C. Ford, Coord. Chem. Rev. 5 (1970) 75.
[75] H. Taube, Pure Appl. Chem. 51 (1979) 901.
[76] C.M.P. Marques, Ph.D Thesis, Instituto de Quimica de Araraquara, UNESP, Araraquara, SP, Brasil, 1993.
[77] C.M.P. Marques, D.W. Franco, R. Sanches, Síntese e Caracterização do íons complexos $[Ru(NH_3)_5pz]^{2+}$ e trans-$[Ru(NH_3)_4SO_2H_2O]^{2+}$ ocluídos na zeólita NaY, in: XIV Simposio Iberoamericano de Catalisis, Chile, 1994, p. 683.
[78] M. Goldwasser, J.F. Dutel, C. Naccache, Zeolites 9 (1989) 54.
[79] P.J. Carl, S.C. Larsen, J. Catal. 196 (2000) 352.
[80] C.W. Clavier, D.L. Rodman, J.F. Sinski, L.R. Allain, H.J. Im, Y. Yang, J.C. Clark, Z.L. Xue, J. Mater. Chem. 15 (2005) 2356.
[81] D.B. Mitzi, Chem. Mater. 13 (2001) 3283.
[82] N.A. Peppas, P. Bures, W. Leobandung, H. Ichikawa, Eur. J. Pharm. Biopharm. 50 (2000) 27.
[83] E.O. Oh, R.K. Gupta, C.M. Whang, J. Sol-Gel Sci. Technol. 28 (2003) 279.
[84] V.S. Tripathi, V.B. Kandimalla, H.X. Ju, Sens. Actuators B-Chem. 114 (2006) 1071.
[85] R. Gupta, N.K. Chaudhury, Biosens. Bioelectron. 22 (2007) 2387.
[86] R.S. da Silva, M.S.P. Marchesi, K. Chosu, C.N. Lunardi, L.M. Bendhack, P.C. Ford, J. Phys. Chem. B 111 (2007) 6962.
[87] A.J. Gomes, A.S. Faustino, C.N. Lunardi, L.O. Lunardi, A.E.H. Machado, Int. J. Pharm. 332 (2007) 153.
[88] A.J. Gomes, L.O. Lunardi, J.M. Marchetti, C.N. Lunardi, A.C. Tedesco, Photomed. Laser Surg. 24 (2006) 514.
[89] A.J. Gomes, L.O. Lunardi, J.M. Marchetti, C.N. Lunardi, A.C. Tedesco, Drug Deliv. 12 (2005) 159.
[90] H.J. Mok, T.G. Park, Eur. J. Pharm. Biopharm. 68 (2008) 105.
[91] A.L. Doiron, K.A. Homan, S. Emelianov, L. Brannon-Peppas, Pharm. Res. 26 (2009) 674.
[92] S. Demir, A. Ogan, N. Kayaman-Apohan, Polym. Int. 57 (2008) 372.
[93] J.F. Xu, Y.S. Wang, Y. Li, X.M. Yang, P. Zhang, H.Y. Hou, Y.Y. Shi, C.X. Song, J. Ocul. Pharmacol. Ther. 23 (2007) 527.
[94] M.L. Hans, A.M. Lowman, Curr. Opin. Solid State Mater. Sci. 6 (2002) 319.
[95] R.A. Jain, Biomaterials 21 (2000) 2475.
[96] D.J. Bharali, V. Pradhan, G. Elkin, W. Qi, A. Hutson, S.A. Mousa, Y. Thanavala, Nanomedicine 4 (2008) 311.
[97] D.J. Kirby, I. Rosenkrands, E.M. Agger, P. Andersen, A.G.A. Coombes, Y. Perrie, J. Drug. Target 16 (2008) 282.
[98] R.C. Mundargi, V.R. Babu, V. Rangaswamy, P. Patel, T.M. Aminabhavi, J. Control. Release 125 (2008) 193.
[99] R. Jalil, J.R. Nixon, J. Microencapsul. 7 (1990) 297.
[100] C. Huabing, M. Dongsheng, D. Danrong, C. Xueling, Z. Dandan, L. Jie, X. Huibi, Y. Xiangliang, Int. J. Pharm. 341 (2007) 78.
[101] Y. Özsoy, S. Güngör, E. Cevher, Il Farmaco 59 (2004) 563.
[102] D.A.C.S. de Santana, R.S. da Silva, Int. J. Pharm. Sci., submitted for publication.
[103] J.A.V. Santos, in preparation.
[104] F.E. Mabbs, M. Collinson, Electron Paramagnetic Resonance of d Transition Metal Compounds, Elsevier, Amsterdam, 1992.
[105] B.R. McGarvey, Quimica Nova 21 (1998) 206.
[106] B.R. McGarvey, Coord. Chem. Rev. 170 (1998) 75.
[107] J.R. Pilbrow, Transition Ion Electron Paramagnetic Resonance, Oxford University Press, New York, 1990.
[108] M.M.T. Khan, A. Hussain, M.A. Moiz, Polyhedron 11 (1992) 687.
[109] G. Socrates, Infrared and Raman Characteristic Group Frequencies: Tables and Charts, J. Wiley, Chichester, 2001.
[110] L.T. Kubota, Y. Gushikem, J. Perez, A.A. Tanaka, Langmuir 11 (1995) 1009.
[111] M.G. Gomes, C.U. Davanzo, S.C. Silva, L.G.F. Lopes, P.S. Santos, D.W. Franco, J. Chem. Soc.-Dalton Trans. (1998) 601.
[112] K.Q. Ferreira, Ph.D. Thesis, Departamento de Quimica da Faculdade de Filosofia, Ciências e Letras de Ribeirão Preto, Universidade de São Paulo, Ribeirão Preto, SP, Brasil, 2004.
[113] R.M. Silverstein, D.J. Kiemle, F.X. Webster, Spectrometric Identification of Organic Compounds, John Wiley & Sons, Hoboken, 2005.

[114] S.E. Mazzetto, L.M.D. Plicas, E. Tfouni, D.W. Franco, Inorg. Chem. 31 (1992) 516.
[115] K. Nakamoto, Infrared and Raman Spectra of Inorganic and Coordination Compounds, Wiley, New York, 1997.
[116] K. Torigoe, A. Suzuki, K. Esumi, J. Colloid Interface Sci. 241 (2001) 346.
[117] P.G. Zanichelli, A.M. Miotto, H.F.G. Estrela, F.R. Soares, D.M. Grassi-Kassisse, R.C. Spadari-Bratfisch, E.E. Castellano, F. Roncaroli, A.R. Parise, J.A. Olabe, A.R.M.S. de Brito, D.W. Franco, J. Inorg. Biochem. 98 (2004) 1921.
[118] S.S. Isied, H. Taube, Inorg. Chem. 15 (1976) 3070.
[119] S.S. Isied, H. Taube, J. Am. Chem. Soc. 95 (1973) 8198.
[120] R.E. Shepherd, A. Proctor, W.W. Henderson, T.K. Myser, Inorg. Chem. 26 (1987) 2440.
[121] J.N.H. Reek, D. Groot, G.E. Oosterom, P.C.J. Kamer, P.W.M.N. Leeuwen, Chimie 6 (2003) 1061.
[122] T. Matsubara, P.C. Ford, Inorg. Chem. 15 (1976) 1107.
[123] D.R. Carmo, Y. Gushikem, D.W. Franco, Spectroscppy and electrochemical properties of $[(CN)_5Ru(CN)Ru(NH_3)_5]$-anchored in thin films of Ti(IV) oxide dispersed on the silica gel surface, in: J.P. Blitz, C.B. Little (Eds.), Fundamental and Applied Aspects of Chemically Modified Surfaces, The Royal Chemical Society, 1999.
[124] D. Guenzburger, A. Garner, J. Danon, Inorg. Chim. Acta 21 (1977) 119.
[125] T. Matsubara, P.C. Ford, Inorg. Chem. 17 (1978) 1747.
[126] P.C. Ford, D.F.P. Rudd, R. Gaunder, H. Taube, J. Am. Chem. Soc. 90 (1968) 1187.
[127] M.L. Bento, E. Tfouni, Inorg. Chem. 27 (1988) 3410.
[128] E. Tfouni, Coord. Chem. Rev. 196 (2000) 281.
[129] E. Tfouni, K.Q. Ferreira, F.G. Doro, R.S. da Silva, Z.N. da Rocha, Coord. Chem. Rev. 249 (2005) 405.
[130] G.N. Coleman, J.W. Gesler, F.A. Shirley, J.R. Kuempel, Inorg. Chem. 12 (1973) 1036.
[131] H.S. Lim, D.J. Barclay, F.C. Anson, Inorg. Chem. 11 (1972) 1460.
[132] J.F. Endicott, H. Taube, J. Am. Chem. Soc. 84 (1962) 4984.
[133] S.R. Wecksler, A. Mikhailovsky, D. Korystov, P.C. Ford, J. Am. Chem. Soc. 128 (2006) 3831.
[134] P.C. Ford, S. Wecksler, Coord. Chem. Rev. 249 (2005) 1382.
[135] M.J. Rose, P.K. Mascharak, Curr. Opin. Chem. Biol. 12 (2008) 238.
[136] M.J. Rose, N.L. Fry, R. Marlow, L. Hinck, P.K. Mascharak, J. Am. Chem. Soc. 130 (2008) 8834.
[137] G.M. Halpenny, P.K. Mascharak, Inorg. Chem. 48 (2009) 1490.
[138] A.A. Eroy-Reveles, Y. Leung, C.M. Beavers, M.M. Olmstead, P.K. Mascharak, J. Am. Chem. Soc. 130 (2008) 4447.
[139] M.J. Rose, P.K. Mascharak, Coord. Chem. Rev. 252 (2008) 2093.
[140] P.C. Ford, J. Bourassa, K. Miranda, B. Lee, I. Lorkovic, S. Boggs, S. Kudo, L. Laverman, Coord. Chem. Rev. 171 (1998) 185.
[141] S. Wecksler, A. Mikhailovsky, P.C. Ford, J. Am. Chem. Soc. 126 (2004) 13566.
[142] S.R. Wecksler, J. Hutchinson, P.C. Ford, Inorg. Chem. 45 (2006) 1192.
[143] K.M. Padden, J.F. Krebs, C.E. MacBeth, R.C. Scarrow, A.S. Borovik, J. Am. Chem. Soc. 123 (2001) 1072.
[144] J. Bordini, D.L. Hughes, J.D.D. Neto, C.J. da Cunha, Inorg. Chem. 41 (2002) 5410.
[145] P.C. Ford, I.M. Lorkovic, Chem. Rev. 102 (2002) 993.
[146] P.C. Ford, Acc. Chem. Res. 41 (2008) 190.
[147] J. Bordini, D.O. Novaes, I.E. Borissevitch, B.T. Owens, P.C. Ford, E. Tfouni, Inorg. Chim. Acta 361 (2008) 2252.
[148] L.M. Bendhack, C.Z. Ferezin, F.S. Oliveira, C.N. Lunardi, A.R. Simioni, A.C. Tedesco, R.S. Silva, FASEB J. 19 (2005) A1553.
[149] R.M. Carlos, A.A. Ferro, H.A.S. Silva, M.G. Gomes, S.S.S. Borges, P.C. Ford, E. Tfouni, D.W. Franco, Inorg. Chim. Acta 357 (2004) 1381.
[150] V. Togniolo, R.S. da Silva, A.C. Tedesco, Inorg. Chim. Acta 316 (2001) 7.
[151] M.G. Sauaia, R.G. de Lima, A.C. Tedesco, R.S. da Silva, J. Am. Chem. Soc. 125 (2003) 14718.
[152] Z.N. da Rocha, R.G. de Lima, F.G. Doro, E. Tfouni, R.S. da Silva, Inorg. Chem. Commun. 11 (2008) 737.
[153] D. Neuman, A.D. Ostrowski, R.O. Absalonson, G.F. Strouse, P.C. Ford, J. Am. Chem. Soc. 129 (2007) 4146.
[154] D. Neuman, A.D. Ostrowski, A.A. Mikhailovsky, R.O. Absalonson, G.F. Strouse, P.C. Ford, J. Am. Chem. Soc. 130 (2008) 168.